

# Nonthermal Two Component Dark Matter Model for Fermi-LAT $\gamma$ -ray excess and 3.55 keV X-ray Line

Anirban Biswas<sup>† 1</sup>, Debasish Majumdar<sup>† 2</sup>, Probir Roy<sup>‡ 3</sup>

<sup>†</sup> *Astroparticle Physics and Cosmology Division,  
Saha Institute of Nuclear Physics, Kolkata 700064, India*

<sup>‡</sup> *Saha Institute of Nuclear Physics, Kolkata 700064, India*

*&*

*Centre for Astroparticle Physics and Space science,  
Bose Institute, Kolkata 700091, India*

## ABSTRACT

A two component model of nonthermal dark matter is formulated to simultaneously explain the Fermi-LAT results indicating a  $\gamma$ -ray excess observed from our Galactic Centre in the 1-3 GeV energy range and the detection of an X-ray line at 3.55 keV from extragalactic sources. Two additional Standard Model singlet scalar fields  $S_2$  and  $S_3$  are introduced. These fields couple among themselves and with the Standard Model Higgs doublet  $H$ . The interaction terms among the scalar fields, namely  $H$ ,  $S_2$  and  $S_3$ , are constrained by the application of a discrete  $\mathbb{Z}_2 \times \mathbb{Z}'_2$  symmetry which breaks softly to a remnant  $\mathbb{Z}''_2$  symmetry. This residual discrete symmetry is then spontaneously broken through an MeV order vacuum expectation value  $u$  of the singlet scalar field  $S_3$ . The resultant physical scalar spectrum has the Standard Model like Higgs as  $\chi_1$  with  $M_{\chi_1} \sim 125$  GeV, a moderately heavy scalar  $\chi_2$  with  $50 \text{ GeV} \leq M_{\chi_2} \leq 80 \text{ GeV}$  and a light  $\chi_3$  with  $M_{\chi_3} \sim 7$  keV. There is only tiny mixing between  $\chi_1$  and  $\chi_2$  as well as between  $\chi_1$  and  $\chi_3$ . The lack of importance of domain wall formation in the present scenario from the spontaneous breaking of the discrete symmetry  $\mathbb{Z}''_2$ , provided  $u \leq 10$  MeV, is pointed out. We find that our proposed two component dark matter model is able to explain successfully both the above mentioned phenomena – the Fermi-LAT observed  $\gamma$ -ray excess (from the  $\chi_2 \rightarrow b\bar{b}$  decay mode) and the observation of the X-ray line (from the decay channel  $\chi_3 \rightarrow \gamma\gamma$ ) by the XMM-Newton observatory.

---

<sup>1</sup>email: anirban.biswas@saha.ac.in

<sup>2</sup>email: debasish.majumdar@saha.ac.in

<sup>3</sup>email: probirrana@gmail.com

# 1 Introduction

The presence of Dark Matter (DM) in the Universe is now an accepted reality. So far, its existence has been inferred only from its gravitational effects. The latter include rotation curves of galaxies, gravitational lensing, observations of the Bullet cluster etc. However, a very attractive proposition is that DM consists of Weakly Interacting Massive Particles (WIMPs) [1] and this is the paradigm that we adopt. The possibility of detecting DM WIMPs through direct and indirect processes is now being vigorously pursued by experimenters. Meanwhile, the amount of DM present in the Universe has been precisely determined by means of results from the PLANCK satellite [2] whose instruments have probed and analysed anisotropies in the smooth cosmic microwave background. One can think of two possible scenarios for the production of DM particles in the early Universe. (1) This could have been due to thermal processes with Standard Model particles interacting with the thermal plasma in the expanding soup ball whereby all possible particle-antiparticle pairs were produced in a reverse chemical process. The decoupling of the DM particles occurred when their interaction rates fell short of the expansion rate of the Universe. Being out of equilibrium, the dark matter particles “froze” to a particular relic density. (2) The DM particles could have originated nonthermally. In this mode, they got produced from out of equilibrium decays of heavier particles. That could have occurred at the stage of the preheating of the Universe from the inflaton energy.

Dark Matter, if accumulated in considerable measure at highly dense regions of celestial bodies, such as at the Galactic Centre (GC) or other sites in a galaxy, may undergo self annihilation. That would lead to high energy photons or fermion-antifermion pairs. Such hard photons may also arise from the radiative decay of a metastable DM particle such as a sterile neutrino or a scalar. Therefore, the observation and analysis of such high energy photons could not only lead to an indirect detection of DM particles but also provide insights into the physics of Dark Matter.

Recently, there have been two major observations of such high energy photons:  $\gamma$ -rays from the centre of our Milky Way galaxy and X-rays from other galaxies and galaxy clusters. The observation of a weak unidentified line in the X-ray spectrum obtained from the XMM-Newton observatory, has been reported by Bulbul et al [3], from an analysis of data from 73 galaxy clusters including Perseus and others. It is also reported in same article [3] that the best fit value of the observed X-ray flux obtained from the XMM-Newton MOS(PN) observation is  $4.0^{+0.8}_{-0.8} \times 10^{-6} (3.9^{+0.6}_{-1.0} \times 10^{-6})$  photons  $\text{cm}^{-2} \text{s}^{-1}$  while the energy of the X-ray line is  $E = 3.57 \pm 0.02 (3.51 \pm 0.03)$  keV. This has been confirmed later by Boyarsky et al [4]. In Ref. [4] this 3.55 keV line has been claimed to have been observed from the Andromeda as well as other galaxies in the Local Group. Separately, analyses of the Fermi-LAT data by several groups [5]-[14] during the last few years have been indicating the presence of a significant excess at an energy

range 1-3 GeV in the  $\gamma$ -ray spectrum observed from regions close to the centre of our Milky way galaxy. There have been attempts to explain the 3.55 keV line from other astrophysical processes. For example, in Ref. [15] the authors claimed from their analysis of XMM-Newton data that a 3.55 keV line from the Galactic Centre could be interpreted from a known plasma line of astrophysical origin. In another work by Carlson et. al. [16] the 3.55 keV line from the Perseus cluster is related to the cool core of the cluster. There have also been attempts [17] to obtain the XMM-Newton X-ray emission line from dwarf galaxies. Authors have considered sterile neutrino dark matter to explain the signature of this emission and accordingly have given upper bounds on the mixing angle of the relevant sterile neutrino DM. X-ray emission lines of the order of 3.5 keV have also been probed from galaxy clusters, the Galactic Centre and M31 where analyses [18] have been made considering sterile neutrino dark matter with a few keV mass. But the authors could not report any  $\sim 3.5$  keV excess. For the case of the 1-3 GeV  $\gamma$ -ray excess from the Galactic Centre, the authors of Ref. [19] attempted to demonstrate the origin of the spectral and the angular features of this excess from inverse compton scattering of high energy electrons available from a burst event in the distant past. A possible millisecond pulsar origin of this  $\gamma$ -ray excess from the Galactic Centre has been discussed in Ref. [20]. But none of the above interpretations has addressed both the phenomena of the X-ray line and the  $\gamma$ -ray excess together. Hence it is natural to conjecture a common origin of both phenomena from processes involving DM particles. There have been many dark matter models in the literature explaining either the Fermi-LAT observed  $\gamma$ -ray excess [21]-[43] or the X-ray line [44]-[68] detected by the XMM-Newton observatory. However, we are among the first two [69] to propose a new single dark matter model explaining both the phenomena simultaneously, although our model of two SM-singlet scalars is very different from that of Ref. [69]. While our explanation of the  $\gamma$ -ray excess is new, our explanation of the X-ray line uses the same mechanism as that of Ref. [57]. Once again, there have been previous works on two component dark matter models [41], [70]-[74], however none of those has been aimed at explaining the Fermi-LAT  $\gamma$ -ray excess and the 3.55 keV X-ray line simultaneously like we do.

In this work we propose a single two-component model for nonthermal dark matter applying it to two completely different parts of the electromagnetic spectrum. We have two distinct scalar dark matter particles, one being light and hence “warm” ( $\sim 7$  keV in mass) and another which is moderately heavy and “cold”, being in the mass range 50–80 GeV. Thus, we extend the scalar sector of the Standard Model (SM) of particle physics by two real scalar field  $S_2$  and  $S_3$ , both of which are singlets under the Standard Model gauge group  $SU(2)_L \times U(1)_Y$ . We envisage nonthermal WIMPs and propose that both the DM particles were produced from decays of the Standard Model Higgs boson as well as from the pair annihilation of SM particles such as fermions, gauge bosons and Higgs bosons. The production processes of these DM particles took place in

the early stage of the Universe when its temperature fell below the electroweak phase transition scale. We need not consider the chemical equilibrium in the thermal bath before electroweak symmetry breaking but are concerned with the nonthermal processes occurring afterwards that lead to the creation of the two lighter scalars. The interactions of the new scalar fields  $S_2, S_3$  – among themselves as well as with the SM Higgs field  $H$  – are controlled by appropriate discrete symmetries which are softly broken down to a residual  $\mathbb{Z}_2''$  symmetry under which both  $S_2$  and  $S_3$  are odd while all other fields are even. This residual discrete symmetry gets spontaneously broken when  $S_3$  develops a Vacuum Expectation Value (VEV)  $u$  of order MeV. This results in a  $3 \times 3$  mass squared matrix in the three dimensional space of the residual neutral SM Higgs field and the two new singlet scalar fields. The diagonalisation of that mass squared matrix leads to three physical scalar masses which are taken as  $M_{\chi_1} \sim 125$  GeV,  $M_{\chi_2} \sim 50$ -80 GeV and  $M_{\chi_3} \sim 7$  keV corresponding respectively to the SM-like Higgs  $\chi_1$  and the two DM particles  $\chi_2$  and  $\chi_3$ <sup>4</sup>.

The comoving number densities  $Y_{\chi_2}$  and  $Y_{\chi_3}$  of  $\chi_2, \chi_3$  at the present epoch are calculated by numerically solving the corresponding two coupled Boltzmann equations describing their temperature evolution. These equations take into the account the roles played by the decays  $\chi_1 \rightarrow \chi_j \chi_j$  ( $j = 2, 3$ ) as well as the pair annihilation processes  $x\bar{x} \rightarrow \chi_j \chi_j$  where  $x$  can be  $W^\pm, Z, f(\bar{f}), \chi_1, \chi_2, f$  being any SM fermion. The individual relic densities  $\Omega_{\chi_2} h^2$  and  $\Omega_{\chi_3} h^2$  at the present temperature then follow in a straightforward way once the above are computed. The temperature variation of these, as well as of the total relic density  $\Omega_T h^2$ , are numerically studied for three cases:  $\Omega_{\chi_2} > \Omega_{\chi_3}$ ,  $\Omega_{\chi_2} < \Omega_{\chi_3}$  and  $\Omega_{\chi_2} \sim \Omega_{\chi_3}$ . The dependence on the mass  $M_{\chi_2}$ , which is not pinpointed, is also studied. The total relic density is always found to lie in the range  $0.1172 \leq \Omega_T h^2 \leq 0.1226$  in conformity with the latest PLANCK results [2].

We further consider the issue of domain wall formation from the restoration of the discrete symmetry  $\mathbb{Z}_2''$  and argue, *à la* Babu and Mahapatra [57], to conclude that the corresponding energy density would be too little to have any effect on the possible overclosing of the Universe or the near-isotropy of the CMB so long as  $u$  is bounded from above by  $\sim 10$  MeV. Finally, we take up the two main issues towards which this paper is addressed: the  $\gamma$ -ray excess observed by Fermi-LAT at 1-3 GeV energies from our GC and the detection of an anomalous 3.55 keV X-ray line from extragalactic sources by the XMM Newton observatory. For the former, we argue that  $\chi_2 \rightarrow b\bar{b}$  is the dominant decay mode acting as a source of GeV energy  $\gamma$ -rays from decays of neutral pions created during the hadronisation of the  $b$  and the  $\bar{b}$ . The computation of the resultant  $\gamma$ -ray flux from the decay of the dark matter candidate  $\chi_2$  is carried through using

---

<sup>4</sup>This mass range for the dark matter component  $\chi_2$  is required to explain the Fermi-LAT excess  $\gamma$ -rays from the decay channel  $\chi_2 \rightarrow b\bar{b}$  (*cf.* Section 6 for a more detailed discussion) while the mass of the other DM component  $\chi_3$  needs to be 7.1 keV so that its decay  $\chi_3 \rightarrow \gamma\gamma$  produces two monoenergetic photons each with energy 3.55 keV.

the NFW [75] halo profile near the GC. A comparison with the Fermi-LAT data provides an excellent fit for the mass range of  $\chi_2$  chosen by us. The observed 3.55 keV X-ray line arises in our model from the decay  $\chi_3 \rightarrow \gamma\gamma$ . We first compute the partial decay width  $\Gamma_{\chi_3 \rightarrow \gamma\gamma}$  of the DM particle  $\chi_3$  utilising three operative one loop diagrams. This partial decay width of  $\chi_3$  for the channel  $\chi_3 \rightarrow \gamma\gamma$ , however, needs to be modified by the factor  $\frac{\Omega_{\chi_3}}{\Omega_T}$  for the purpose of computing the differential X-ray flux since we are working in a multicomponent dark matter scenario. We find that the modified decay width for the channel  $\chi_3 \rightarrow \gamma\gamma$  lies within the range predicted in Refs. [3, 4, 66] so long as the VEV  $u$  of the singlet scalar field  $S_3$  is bounded from below by 2.4 MeV. The decay modes  $\chi_2 \rightarrow b\bar{b}$  and  $\chi_3 \rightarrow \gamma\gamma$  arise respectively through the nonzero mixing of both the dark matter candidates  $\chi_2$  and  $\chi_3$  with the SM-like Higgs boson  $\chi_1$ . Moreover, the  $\chi_1\chi_2\chi_2$  and  $\chi_1\chi_3\chi_3$  couplings are sufficiently small (owing to the nonthermal origin of  $\chi_2$  and  $\chi_3$ ) to evade all the existing constraints from dark matter detection experiments [76, 77].

The rest of the paper is organised as follows. In Section 2 we describe the model and discuss its interscalar interactions as well as the emergent  $3 \times 3$  mass squared matrix in the scalar sector. Section 3 presents the calculation of the relic densities  $\Omega_{\chi_2} h^2$ ,  $\Omega_{\chi_3} h^2$  at the present temperature and a discussion of their variation with temperature. In Section 4 we discuss the issue of possible domain wall formation and point out why it is unimportant in the present context. The spin independent elastic scattering cross sections of both the dark matter particles are computed in Section 5. Section 6 contains our calculation of the  $\gamma$ -ray flux arising from the decay of the dark matter component  $\chi_2$  and its comparison with the available Fermi-LAT data. In Section 7 we compute the decay width  $\Gamma_{\chi_3 \rightarrow \gamma\gamma}$  for the channel  $\chi_3 \rightarrow \gamma\gamma$  which is required to produce the observed 3.55 keV X-ray line from the decay of the dark matter particle  $\chi_3$ . The final Section 8 summarises our conclusions. The two appendices (A.1 and A.2) contain the algebraic expressions for the couplings and masses of the physical scalars  $\chi_1$ ,  $\chi_2$  and  $\chi_3$ .

## 2 The Model

We start with the Standard Model fields including, in particular, the  $SU(2)_L$  Higgs doublet

$$H = \begin{pmatrix} h^+ \\ \frac{s_1 + ip_1 + v}{\sqrt{2}} \end{pmatrix}. \quad (1)$$

Here  $s_1$  is the residual neutral SM Higgs field,  $h^+$  and  $p_1$  are unphysical charged and neutral pseudoscalar Higgs fields while  $v$  is the Vacuum Expectation Value  $\simeq 246$  GeV. Thus

$$\langle H \rangle = \begin{pmatrix} 0 \\ \frac{v}{\sqrt{2}} \end{pmatrix}. \quad (2)$$

Our DM sector consists of two real scalar fields  $S_2$  and  $S_3$  which are singlets under the SM gauge group  $SU(2)_L \times U(1)_Y$ . The Lagrangian of the spin zero sector of the present model can then be written in terms of the  $SU(2)_L \times U(1)_Y$  gauge covariant derivative  $D_\mu$  and a scalar potential function  $V(H, S_2, S_3)$ :

$$\mathcal{L} = (D_\mu H)^\dagger (D^\mu H) + \frac{1}{2} \partial_\mu S_2 \partial^\mu S_2 + \frac{1}{2} \partial_\mu S_3 \partial^\mu S_3 - V(H, S_2, S_3) . \quad (3)$$

The stability of the newly added scalars  $S_{2,3}$  is ensured by the postulated invariance of the model under the discrete symmetry  $\mathbb{Z}_2 \times \mathbb{Z}'_2$  with respect to which only these two fields transform nontrivially. The  $\mathbb{Z}_2 \times \mathbb{Z}'_2$  charges of  $S_2$  and  $S_3$  are  $(-1, 1)$  and  $(1, -1)$  respectively, whereas the corresponding charge of every other field in the model is  $(1, 1)$ . Thus, while  $S_2$  ( $S_3$ ) is odd (even) under  $\mathbb{Z}_2$ , the reverse is the case for  $S_2$  ( $S_3$ ) with respect to  $\mathbb{Z}'_2$ . The function  $V(H, S_2, S_3)$  of Eq. (3) contains all possible  $\mathbb{Z}_2 \times \mathbb{Z}'_2$  invariant interaction terms among the Standard Model Higgs doublet field  $H$  and the singlet fields  $S_2, S_3$  including all allowed self interactions and mass terms. We write it explicitly in Eq. (4):

$$\begin{aligned} V(H, S_2, S_3) = & \kappa_1 \left( H^\dagger H - \frac{v^2}{2} \right)^2 + \frac{\kappa_2}{4} S_2^4 + \frac{\kappa_3}{4} (S_3^2 - u^2)^2 + \frac{\rho_2^2}{2} S_2^2 + \lambda_{12} (H^\dagger H) S_2^2 + \lambda_{23} S_2^2 S_3^2 \\ & + \lambda_{13} \left( H^\dagger H - \frac{v^2}{2} \right) (S_3^2 - u^2) . \end{aligned} \quad (4)$$

The required invariance under the symmetry  $\mathbb{Z}_2 \times \mathbb{Z}'_2$  excludes terms such as  $(H^\dagger H) S_2 S_3$ ,  $S_2^3 S_3$ ,  $S_2 S_3^3$ . We also assume that, due to high scale physics, a ‘soft’ term

$$V' = \alpha S_2 S_3 \quad (5)$$

gets added to  $V$ , explicitly breaking the  $\mathbb{Z}_2 \times \mathbb{Z}'_2$  invariance down to  $\mathbb{Z}''_2$  under which both  $S_2$  and  $S_3$  are odd. We have introduced six ‘hard’ couplings in  $V$  –  $\kappa_{1,2,3}$ , and  $\lambda_{12}, \lambda_{23}, \lambda_{13}$  – all of which describe quartic field interactions in their leading terms. Besides the six quartic couplings, we have also a dimensional coupling  $\rho_2$ . The nonleading terms in the potential  $V$  have been chosen in a way that  $V$  is manifestly minimised at  $\langle H \rangle = \frac{v}{\sqrt{2}}$ ,  $\langle S_2 \rangle = 0$ ,  $\langle S_3 \rangle = u$ . The VEV  $u$  needs to be in the range  $2 \text{ MeV} < u \leq 10 \text{ MeV}$  (see Sections 4, 7 for details). As a result, the residual discrete symmetry  $\mathbb{Z}''_2$  gets spontaneously broken. The stability of the potential  $V$  in Eq. (4) can be investigated following the procedure of Ref. [78]. The required conditions are:

$$\kappa_{1,2,3} > 0 , \quad (6)$$

$$\rho_2 > 0 , \quad (7)$$

$$\lambda_{12} + \sqrt{\kappa_1 \kappa_2} > 0 , \quad (8)$$

$$\lambda_{13} + \sqrt{\kappa_1 \kappa_3} > 0 , \quad (9)$$

$$\lambda_{23} + \frac{1}{2} \sqrt{\kappa_2 \kappa_3} > 0 , \quad (10)$$

$$\sqrt{2(\lambda_{12} + \sqrt{\kappa_1 \kappa_2})(\lambda_{13} + \sqrt{\kappa_1 \kappa_3})(2\lambda_{23} + \sqrt{\kappa_2 \kappa_3})} + \sqrt{\kappa_1 \kappa_2 \kappa_3} + \lambda_{12}\sqrt{\kappa_3} + \lambda_{13}\sqrt{\kappa_2} + 2\lambda_{23}\sqrt{\kappa_1} > 0. \quad (11)$$

In analogy with the residual neutral SM Higgs field  $s_1$ , we can define the corresponding  $s_2 \equiv S_2$  and  $s_3 = S_3 - u$ . Now, in the  $s_1$ - $s_2$ - $s_3$  system, the squared mass matrix is given by

$$\mathcal{M}^2 = \begin{pmatrix} 2\kappa_1 v^2 & 0 & 2\lambda_{13}uv \\ 0 & \rho_2^2 + \lambda_{12}v^2 + 2\lambda_{23}u^2 & \alpha \\ 2\lambda_{13}uv & \alpha & 2\kappa_3 u^2 \end{pmatrix}. \quad (12)$$

The eigenvalues of  $\mathcal{M}^2$  are designated  $M_{\chi_1}^2$ ,  $M_{\chi_2}^2$  and  $M_{\chi_3}^2$ . The eigenstates, namely the physical scalars  $\chi_1$ ,  $\chi_2$ ,  $\chi_3$ , are linearly related to  $S_1$ ,  $S_2$ ,  $S_3$  by an orthogonal transformation which may be characterised in the usual way by the mixing angles  $\theta_{12}$ ,  $\theta_{23}$  and  $\theta_{13}$ . The latter are the rotation angles needed to rotate the  $S_1$ - $S_2$ ,  $S_2$ - $S_3$  and  $S_3$ - $S_1$  mass squared submatrices ( $2 \times 2$  matrices) sequentially such that the whole mass squared matrix  $\mathcal{M}^2$  (Eq. (12)) becomes diagonal. The approximate expressions for  $M_{\chi_1}^2$ ,  $M_{\chi_2}^2$  and  $M_{\chi_3}^2$  are given in the Appendix A.2. We only note that  $M_{\chi_1} > M_{\chi_2} > M_{\chi_3}$  with  $M_{\chi_1} \sim 125$  GeV,  $M_{\chi_2} \simeq 50 - 80$  GeV and  $M_{\chi_3} \sim 7$  keV.<sup>5</sup>

### 3 Relic Density Calculation of Two Component Nonthermal Dark Matter

In the present scenario both the heavier and lighter dark matter components would be produced nonthermally in the early Universe. We assume that, when the temperature of the Universe was above that of electroweak symmetry breaking, there was no source of production of the DM particles  $\chi_2$  and  $\chi_3$ . After the breaking of  $SU(2)_L \times U(1)_Y$  symmetry, the self-annihilation of SM particles such as W, Z, Higgs, t-quark and/or decays of the Higgs boson act as primary sources of the dark matter particles  $\chi_2$  and  $\chi_3$ . The Feynman diagrams of the above mentioned processes, which are relevant for the evolution of the number densities of  $\chi_2$  and  $\chi_3$ , are shown in Fig. 1. We compute the number densities of both the dark matter components  $\chi_2$  and  $\chi_3$  at the present temperature ( $T_0 \sim 10^{-13}$  GeV) by numerically solving two coupled Boltzmann equations which

---

<sup>5</sup>The light mass  $\mathcal{O}(\text{keV})$  for the dark matter component  $\chi_3$  arises from an order MeV value of  $u$  (*cf.* Sections 4, 7) so long as the parameter  $\kappa_3$  lies in the range  $\sim 2 \times 10^{-7}$  to  $4 \times 10^{-6}$ .

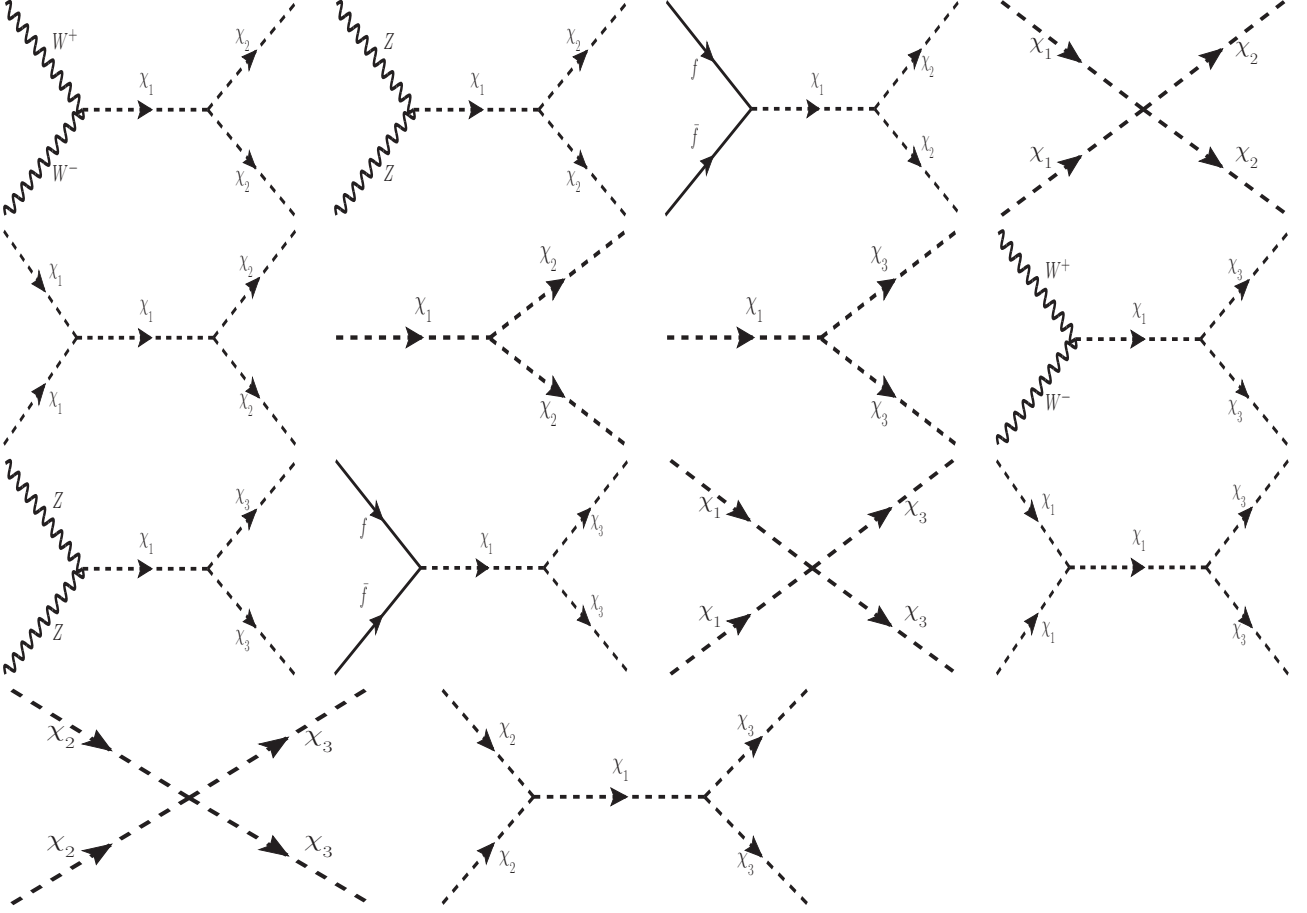


Figure 1: Feynman diagrams for dominant production channels of both the dark matter components  $\chi_2$  and  $\chi_3$

are given below.

$$\begin{aligned}
 \frac{dY_{\chi_2}}{dz} = & -\frac{2M_{pl}}{1.66M_{\chi_1}^2} \frac{z \sqrt{g_*(T)}}{g_s(T)} \left( \langle \Gamma_{\chi_1 \rightarrow \chi_2 \chi_2} \rangle (Y_{\chi_2} - Y_{\chi_1}^{eq}) \right) - \frac{4\pi^2}{45} \frac{M_{pl} M_{\chi_1}}{1.66} \frac{\sqrt{g_*(T)}}{z^2} \times \\
 & \left( \sum_{x=W,Z,f,H} \langle \sigma v_{x\bar{x} \rightarrow \chi_2 \chi_2} \rangle (Y_{\chi_2}^2 - Y_{\chi_1}^{eq\,2}) + \langle \sigma v_{\chi_2 \chi_2 \rightarrow \chi_3 \chi_3} \rangle Y_{\chi_2}^2 \right),
 \end{aligned} \tag{13}$$



$$\begin{aligned} \frac{dY_{\chi_3}}{dz} = & -\frac{2M_{pl}}{1.66M_{\chi_1}^2} \frac{z \sqrt{g_*(T)}}{g_s(T)} \left( \langle \Gamma_{\chi_1 \rightarrow \chi_3 \chi_3} \rangle (Y_{\chi_3} - Y_{\chi_1}^{eq}) \right) - \frac{4\pi^2 M_{pl} M_{\chi_1}}{45 \cdot 1.66} \frac{\sqrt{g_*(T)}}{z^2} \times \\ & \left( \sum_{x=W,Z,f,H} \langle \sigma v_{x\bar{x} \rightarrow \chi_3 \chi_3} \rangle (Y_{\chi_3}^2 - Y_{\chi_1}^{eq\,2}) - \langle \sigma v_{\chi_2 \chi_2 \rightarrow \chi_3 \chi_3} \rangle Y_{\chi_2}^2 \right). \end{aligned} \quad (14)$$

In Eqs. (13) and (14),  $Y_{\chi_2} = \frac{n_{\chi_2}}{s}$  ( $Y_{\chi_3} = \frac{n_{\chi_3}}{s}$ ) is the comoving number density of  $\chi_2$  ( $\chi_3$ ),  $z = \frac{M_{\chi_1}}{T}$  and  $T$  is the photon temperature while  $s$  is the entropy density of the Universe<sup>6</sup>. Here the number densities of  $\chi_2$ ,  $\chi_3$  are denoted by  $n_{\chi_2}$ ,  $n_{\chi_3}$  respectively. Further,  $M_{pl}$  is the Planck mass and  $g_*$  is given by

$$\sqrt{g_*(T)} = \frac{g_s(T)}{\sqrt{g_\rho(T)}} \left( 1 + \frac{1}{3} \frac{d \ln g_s(T)}{d \ln T} \right). \quad (15)$$

In the above,  $g_\rho(T)$  and  $g_s(T)$  are the effective degrees of freedom related to the energy density  $\rho$  and the entropy density  $s$  respectively of the Universe through the relations  $\rho = g_\rho(T) \frac{\pi^2}{30} T^4$ ,  $s = g_s(T) \frac{2\pi^2}{45} T^3$ . Thus  $g_*$  is a function of the stated effective degrees of freedom. The thermal averages of decay widths ( $\Gamma$ ) and annihilation cross sections times relative velocities ( $\sigma v$ ) for various processes, that occur in Eqs. 13 and 14, can be expressed as

$$\langle \Gamma_{\chi_1 \rightarrow \chi_j \chi_j} \rangle = \Gamma_{\chi_1 \rightarrow \chi_j \chi_j} \frac{K_1(z)}{K_2(z)}, \quad j = 2, 3, \quad (16)$$

$$\begin{aligned} \langle \sigma v_{x\bar{x} \rightarrow \chi_j \chi_j} \rangle &= \frac{1}{8M_x^4 T K_2^2\left(\frac{M_x}{T}\right)} \int_{4M_x^2}^{\infty} \sigma_{x\bar{x} \rightarrow \chi_j \chi_j} (s - 4M_x^2) \sqrt{s} K_1\left(\frac{\sqrt{s}}{T}\right) ds, \\ j = 2, 3, \quad x &= W^\pm, Z, f, \chi_1, \chi_2. \end{aligned} \quad (17)$$

In Eqs. (16), (17)  $K_i$  is the modified Bessel function of order  $i$  and  $s$  is the Mandelstam variable. The decay widths  $\Gamma_{\chi_1 \rightarrow \chi_j \chi_j}$  and annihilation cross sections  $\sigma_{x\bar{x} \rightarrow \chi_j \chi_j}$  (for  $j = 2, 3$ ,

---

<sup>6</sup>It is to be noted that in the above two Boltzmann equations (Eqs. (13), (14)) we have neglected a term involving  $\langle \sigma v_{\chi_3 \chi_3 \rightarrow \chi_2 \chi_2} \rangle Y_{\chi_3}^2$ . At an earlier epoch during the initial stage of production of  $\chi_3$  (mainly from the decay of  $\chi_1$ ), the number density of  $\chi_3$  was very low and hence this term could be neglected. On the other hand, at a later epoch when the Universe cools down to a temperature lower than the mass of  $\chi_2$ , the process  $\chi_3 \chi_3 \rightarrow \chi_2 \chi_2$  will not have any significant contribution to the term  $\langle \sigma v_{\chi_3 \chi_3 \rightarrow \chi_2 \chi_2} \rangle Y_{\chi_3}^2$  even though the number density for  $\chi_3$  is higher.

$x = W^\pm, Z, f, \chi_1, \chi_2$ ) of the processes mentioned in the subscripts of  $\Gamma$  and  $\sigma$  are given below:

$$\Gamma_{\chi_1 \rightarrow \chi_j \chi_j} = \frac{g_{\chi_1 \chi_j \chi_j}^2}{8\pi M_{\chi_1}} \sqrt{1 - \frac{4M_{\chi_j}^2}{M_{\chi_1}^2}}, \quad (18)$$

$$\begin{aligned} \sigma_{\chi_1 \chi_1 \rightarrow \chi_j \chi_j} = & \frac{1}{2\pi s} \sqrt{\frac{s - 4M_{\chi_j}^2}{s - 4M_{\chi_1}^2}} \left\{ g_{\chi_1 \chi_1 \chi_j \chi_j}^2 + \frac{9 g_{\chi_1 \chi_1 \chi_1}^2 g_{\chi_1 \chi_j \chi_j}^2}{[(s - M_{\chi_1}^2)^2 + (\Gamma_{\chi_1} M_{\chi_1})^2]} \right. \\ & \left. - \frac{6 g_{\chi_1 \chi_1 \chi_j \chi_j} g_{\chi_1 \chi_1 \chi_1} g_{\chi_1 \chi_j \chi_j} (s - M_{\chi_1}^2)}{[(s - M_{\chi_1}^2)^2 + (\Gamma_{\chi_1} M_{\chi_1})^2]} \right\}, \end{aligned} \quad (19)$$

$$\begin{aligned} \sigma_{\chi_2 \chi_2 \rightarrow \chi_3 \chi_3} = & \frac{1}{2\pi s} \sqrt{\frac{s - 4M_{\chi_3}^2}{s - 4M_{\chi_2}^2}} \left\{ g_{\chi_2 \chi_2 \chi_3 \chi_3}^2 + \frac{g_{\chi_2 \chi_2 \chi_1}^2 g_{\chi_1 \chi_3 \chi_3}^2}{[(s - M_{\chi_1}^2)^2 + (\Gamma_{\chi_1} M_{\chi_1})^2]} \right. \\ & \left. - \frac{2 g_{\chi_2 \chi_2 \chi_3 \chi_3} g_{\chi_2 \chi_2 \chi_1} g_{\chi_1 \chi_3 \chi_3} (s - M_{\chi_1}^2)}{[(s - M_{\chi_1}^2)^2 + (\Gamma_{\chi_1} M_{\chi_1})^2]} \right\}, \end{aligned} \quad (20)$$

$$\sigma_{WW \rightarrow \chi_j \chi_j} = \frac{g_{WW\chi_1}^2 g_{\chi_1 \chi_j \chi_j}^2}{72\pi s} \sqrt{\frac{s - 4M_{\chi_j}^2}{s - 4M_W^2}} \frac{\left(3 - \frac{s}{M_W^2} + \frac{s^2}{4M_W^4}\right)}{(s - M_{\chi_1}^2)^2}, \quad (21)$$

$$\sigma_{ZZ \rightarrow \chi_j \chi_j} = \frac{g_{ZZ\chi_1}^2 g_{\chi_1 \chi_j \chi_j}^2}{18\pi s} \sqrt{\frac{s - 4M_{\chi_j}^2}{s - 4M_Z^2}} \frac{\left(3 - \frac{s}{M_Z^2} + \frac{s^2}{4M_Z^4}\right)}{(s - M_{\chi_1}^2)^2}, \quad (22)$$

$$\sigma_{f\bar{f} \rightarrow \chi_j \chi_j} = \frac{n_c g_{f\bar{f}\chi_1}^2 g_{\chi_1 \chi_j \chi_j}^2}{16\pi s} \frac{\sqrt{(s - 4M_{\chi_j}^2)(s - 4M_f^2)}}{(s - M_{\chi_1}^2)^2}. \quad (23)$$

In the above equations  $g_{ijk}$  and  $g_{ijkl}$  are couplings of the vertices involving the fields  $i, j, k$  as well as  $i, j, k, l$  respectively while  $M_W, M_Z$  and  $M_f$  are the masses of W boson, Z boson and fermion  $f$  ( $f$  is any SM fermion). All the couplings which are necessary to calculate the decay widths and annihilation cross sections are given in the Appendix A.1.

Finally, the total relic density ( $\Omega_{\text{T}} h^2$ ) of dark matter in the Universe is given in terms of the

normalised Hubble constant  $h = \frac{H_o}{100\text{km/Mpc/s}}$  as

$$\Omega_{\text{T}} h^2 = \Omega_{\chi_2} h^2 + \Omega_{\chi_3} h^2 . \quad (24)$$

Once we obtain the comoving number densities  $Y_{\chi_2}(T_0)$ ,  $Y_{\chi_3}(T_0)$  of both the dark matter components  $\chi_2$  and  $\chi_3$  at the present temperature  $T_0$  by numerically solving the two coupled Boltzmann equations (Eqs. 13, 14), the individual relic densities ( $\Omega_{\chi_2} h^2$  and  $\Omega_{\chi_3} h^2$ ) of each of the components can be obtained from [79, 80]

$$\Omega_{\chi_i} h^2 = 2.755 \times 10^8 \left( \frac{M_{\chi_i}}{\text{GeV}} \right) Y_{\chi_i}(T_0) \quad (i = 2, 3) . \quad (25)$$

While solving these two coupled equations (Eqs. (13), (14)), we have adopted the following boundary condition: at the electroweak phase transition temperature, which corresponds to  $z (= \frac{M_{\chi_1}}{T}) \simeq 0.83$ , the number densities of both the dark matter candidates are zero. The plots (a–c) in Fig. 2 show the variation of the relic densities of both the dark matter candidates  $\chi_2$  and  $\chi_3$  with  $z$  (inverse of temperature) for different values of model parameters, namely  $\lambda_{12}$ ,  $\lambda_{13}$ . It is to be noted that these parameters turn out to be of order  $\sim 10^{-9}$ - $10^{-11}$  on account of the smallness of the comoving number density  $Y_{\chi_i}$  required to satisfy the observed dark matter relic density in the Universe. All these plots (a–c) of Fig. 2 are drawn for the case with  $M_{\chi_2} = 70$  GeV and  $M_{\chi_3} = 7.1$  keV. The red solid line in each plot of Fig 2 represents the relic density of the heavier dark matter component ( $\chi_2$ ) while the green and blue solid lines denote the relic densities of the lighter DM candidate  $\chi_3$  and the total density of both the dark matter components respectively. In plot (a) of Fig. 2 we have chosen the values of  $\lambda_{12}$ ,  $\lambda_{13}$  in such a way that the DM particle  $\chi_2$  becomes the dominant component within the dark sector in terms of its contributions towards the total dark matter relic density ( $\Omega_{\text{T}} h^2$ ). However, for the other two plots, different sets of chosen values of  $\lambda_{12}$  and  $\lambda_{13}$  result in the situations where  $\Omega_{\chi_2} h^2 < \Omega_{\chi_3} h^2$  (plot b) and  $\Omega_{\chi_2} h^2 \sim \Omega_{\chi_3} h^2$  (plot c). It appears from each plot of Fig. 2 that the relic density of each dark matter candidate starts growing from an initial value zero (due to the adopted boundary condition discussed earlier), thereafter, as the temperature of the Universe decreases ( $z$  increases), the relic densities of both the DM components increase since more and more dark matter particles are produced by the decay and/or self annihilation of the SM particles. Finally, the relic densities of both the dark matter particles saturate to the respective particular values at  $z \sim 10$  (corresponding to a temperature  $T \sim 12$  GeV of the Universe) which depend upon the values of the parameters  $\lambda_{12}$  and  $\lambda_{13}$ . It is also seen from Fig. 2 that in all three cases the saturation values of the total relic density of the two dark matter candidates always lie within the range  $0.1172 \leq \Omega_{\text{DM}} h^2 \leq 0.1226$ , as predicted by the PLANCK experiment [2] at a 68% C.L. In Fig. 3 we show the variation of the relic density of the heavier dark matter component  $\chi_2$

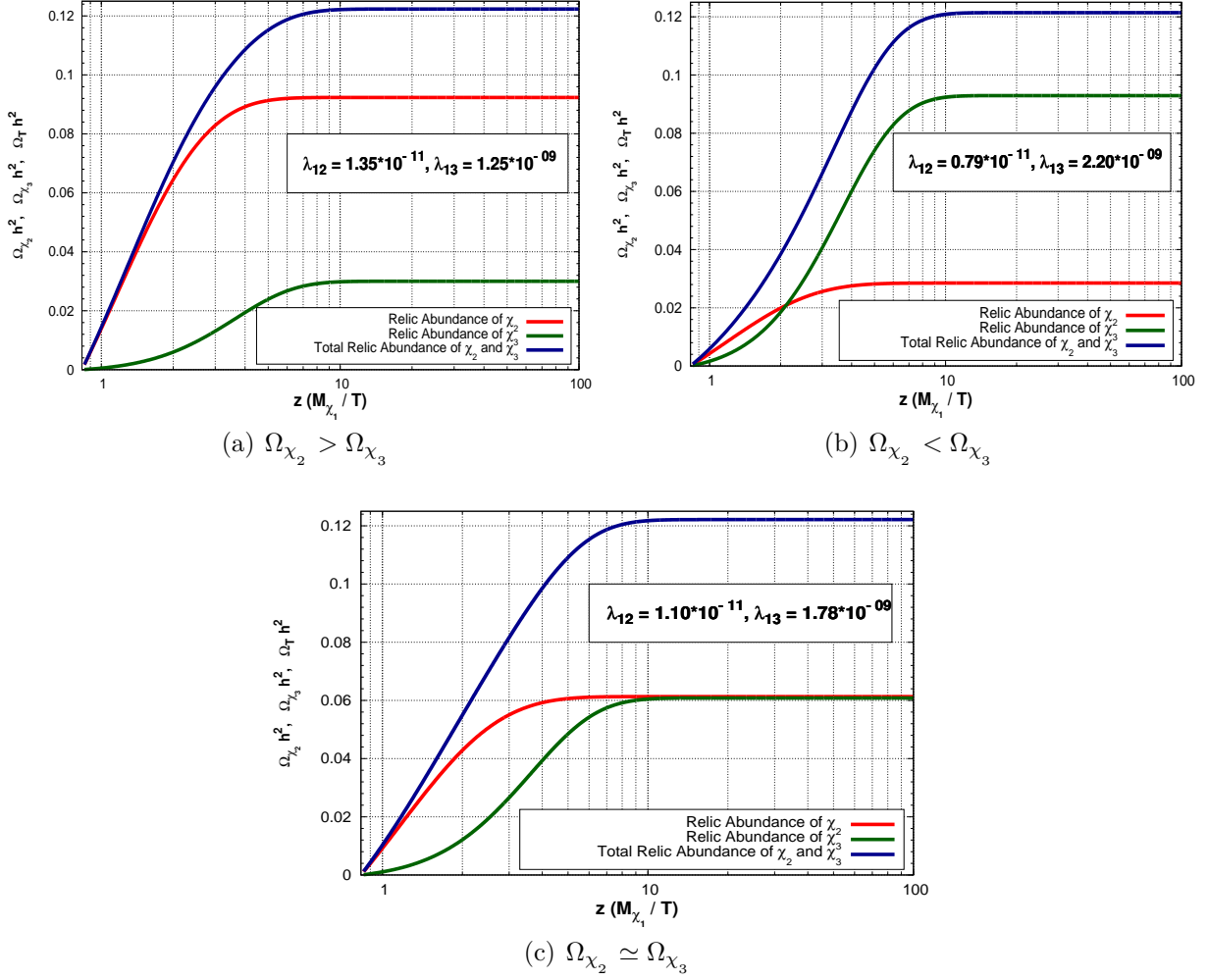


Figure 2: Variation of relic densities of both the dark matter candidates with  $z$ .

with  $z$  for three different values of  $M_{\chi_2} = 65, 70, 80$  GeV with  $\lambda_{12} = 1.10 \times 10^{-11}$ .

In the three plots (a–c) of Fig. 4, we show the allowed regions in the parameter space  $\lambda_{12}$ – $\lambda_{13}$ ,  $\theta_{12}$ – $\theta_{13}$  and  $\theta_{12}$ – $\theta_{23}$  respectively. These plots (a–c of Fig. 4) are drawn for  $50 \text{ GeV} \leq M_{\chi_2} \leq 80 \text{ GeV}$ ,  $M_{\chi_3} = 7.1 \text{ keV}$ ,  $2 \text{ MeV} < u \leq 10 \text{ MeV}$ , and  $10^{-9} \text{ GeV}^2 \lesssim \alpha \lesssim 10^{-7} \text{ GeV}^2$ . The choice of the numerical ranges of these parameters will be justified in Sections 4, 6 and 7. In order to avoid the late time decay of the heavier dark matter particle  $\chi_2$  into two lighter DM component  $\chi_3$ , we adopt the value of the parameter  $\lambda_{23} \leq 10^{-6}$ . The constraint for all the plots of Fig. 4 is that the calculations of relic densities with the allowed values of the parameters must satisfy the PLANCK result for the total relic density of dark matter in the Universe. It is also to be noted that, for plot (a) in Fig. 4, we obtain two allowed regions in the parameter space  $\lambda_{12}$ – $\lambda_{13}$ . The nonthermal production of the present dark matter candidates proceeds through two processes,

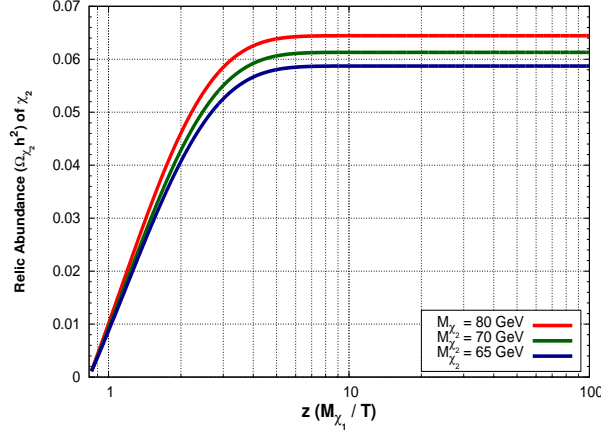


Figure 3: Variation of relic density of the dark matter component  $\chi_2$  with  $z$  for three different values of  $M_{\chi_2} = 65, 70, 80$  GeV.

namely the decay of the SM Higgs and pair annihilation of SM particles. But, if the mass of the heavier dark matter is higher than  $M_{\chi_1}/2$ , then it will not be produced through the decay of the SM Higgs boson. In this case the heavier dark matter can only be produced by the pair annihilation of SM particles. The lower allowed region in plot (a) between  $\lambda_{12}$  and  $\lambda_{13}$  is for the case when the mass of the heavier dark matter is less than  $M_{\chi_1}/2$  while the other region is for the case when the nonthermal production of the same is through the pair annihilation of SM particles. Needless to mention here that the lighter component can always be produced from the decay of the SM Higgs boson. The allowed ranges for the model parameters  $\lambda_{12}$ ,  $\lambda_{13}$ ,  $\theta_{12}$ ,

$\lambda_{12}$	$\lambda_{13}$	$\theta_{12}$ (rad)	$\theta_{13}$ (rad)	$\theta_{23}$ (rad)
$\sim (0.18 - 1.6) \times 10^{-11}$	$\sim (0.56 - 2.6) \times 10^{-9}$	$\sim (0.1 - 2.4) \times 10^{-23}$	$\sim (0.2 - 2.0) \times 10^{-11}$	$\sim (0.5 - 8.0) \times 10^{-13}$

Table 1: Allowed ranges for the model parameters  $\lambda_{12}$ ,  $\lambda_{13}$ ,  $\theta_{12}$ ,  $\theta_{13}$ ,  $\theta_{23}$ .

$\theta_{13}$ ,  $\theta_{23}$ , obtained from the plots a–c of Fig. 4, are given in a tabular form (Table 1). Thus  $\theta_{13}$ ,  $\theta_{23}$  and  $\theta_{12}$  turn out to be very small angles in the range  $\sim 10^{-11}$  rad,  $10^{-13}$  rad and  $10^{-23}$  rad respectively, as the off-diagonal elements of the mass squared matrix of Eq. (12) are constrained to be very small.

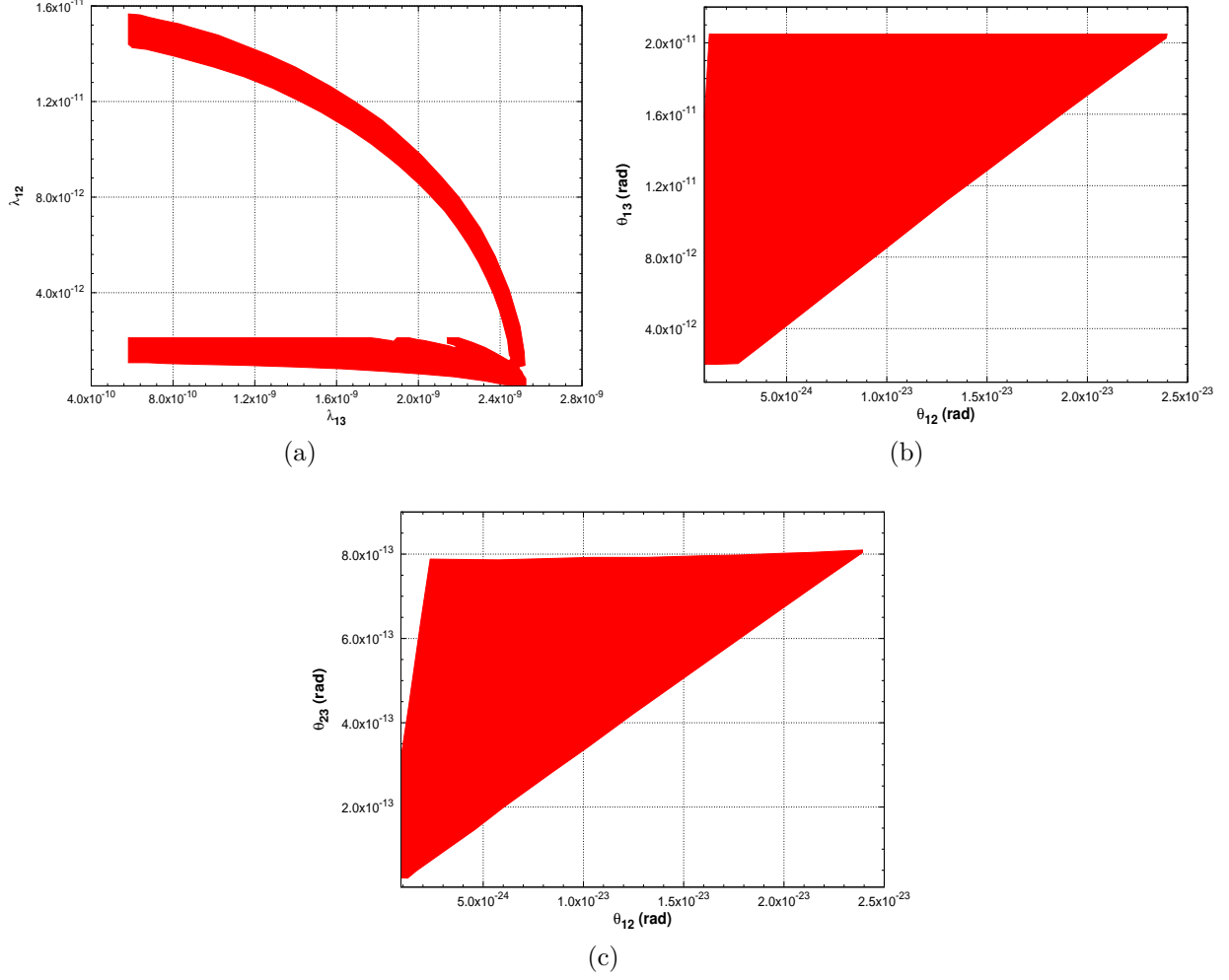


Figure 4: Allowed ranges of model parameters namely,  $\lambda_{12}$ ,  $\lambda_{13}$ ,  $\theta_{12}$ ,  $\theta_{23}$  and  $\theta_{13}$ .

## 4 Domain wall formation from restoration of $\mathbb{Z}_2''$

In this present model, though the residual discrete  $\mathbb{Z}_2''$  symmetry is spontaneously broken by the VEV  $u$  of the scalar field  $S_3$ , there still remains the possibility that the symmetry could be restored at a high temperature. This would result in the formation of domain walls. Since the scalar field  $S_1$  is in thermal equilibrium with the Universe, the interaction between the scalars  $S_1$  and  $S_3$  results in a temperature dependent mass term for the field  $S_3$ . The expression for the temperature dependent mass term  $\mu_{S_3}^2(T)$  is given by [81],

$$\mu_{S_3}^2(T) = \frac{\lambda_{13} T^2}{2\pi^2} \int_0^\infty dx \frac{x^2}{\sqrt{x^2 + M_{S_1}^2/T^2}} \frac{1}{e^{\sqrt{x^2 + M_{S_1}^2/T^2}} - 1}. \quad (26)$$

We are considering the epoch of the Universe when  $T \ll M_{S_1}$ . In this limit, we can write the above equation (Eq. (26)) in the following approximate form

$$\begin{aligned}\mu_{S_3}^2(T) &\simeq \left( \frac{\lambda_{13} M_{S_1} T}{2\pi^2} \right) K_1 \left( \frac{M_{S_1}}{T} \right), \quad T \ll M_h \\ &\simeq \frac{\lambda_{13}}{2\sqrt{2}\pi^2} T^2 \sqrt{\frac{M_{S_1}}{T}} e^{-M_{S_1}/T} \left( 1 + \frac{3}{8} \frac{T}{M_{S_1}} - \frac{15}{128} \frac{T^2}{M_{S_1}^2} + \dots \right).\end{aligned}\quad (27)$$

From Eq. (4) we see that there is a wrong sign mass term  $-\frac{\kappa_3}{2}u^2$  of the field  $S_3$ . Combining this bare mass term with the temperature dependent mass term given in Eq. (26), we can define a quantity which is

$$M_{S_3}^2(T) = \mu_{S_3}^2(T) - \frac{\kappa_3}{2}u^2. \quad (28)$$

The discrete symmetry  $\mathbb{Z}_2''$  will be restored again if the quantity  $M_{S_3}^2(T)$  changes its sign and

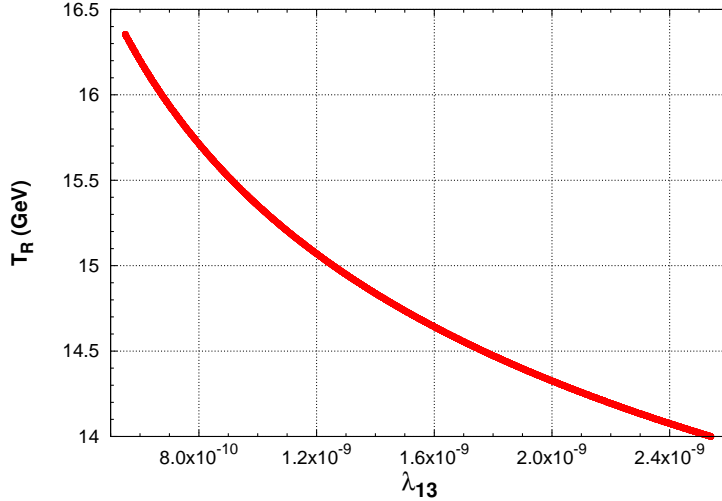


Figure 5: Variation of discrete symmetry ( $\mathbb{Z}_2''$ ) restoration temperature with the parameter  $\lambda_{13}$ .

becomes positive. This will happen only if the quartic coupling  $\lambda_{13}$  between the fields  $S_1$  and  $S_3$  (see Eq. (4)) is positive. For negative values of  $\lambda_{13}$ , which are equally allowed, there is no possibility that the spontaneously broken discrete symmetry  $\mathbb{Z}_2''$  could be restored again. The temperature at which this phase transition occurs is defined as the symmetry restoration temperature  $T_R$ . In Fig. 5, we show the variation of  $T_R$  with the allowed values of the coupling parameter  $\lambda_{13}$ . It is seen from Fig. 5 that for the allowed values of  $\lambda_{13}$ ,  $T_R$  varies from  $\sim 14$  GeV to  $\sim 16.5$  GeV.

We note that our  $T_R$  is quite close to the discrete symmetry restoration temperature  $\sim 15.2$  GeV obtained in the model of Babu and Mahapatra [57]. Therefore, the properties of any domain

wall that is formed here will be similar to theirs. In consequence, their discussion carries over to our case *mutatis mutandis* and the energy density of such a domain wall would be too little either to overclose the Universe or affect the observed near-isotropy of the CMB so long as the VEV  $u$  of the scalar field  $S_3$  is bounded from above by  $\sim 10$  MeV.

## 5 Direct detection of the dark matter candidates $\chi_2$ and $\chi_3$ .

In the present two component dark matter model both the dark matter particles, namely  $\chi_2$  and  $\chi_3$ , scatter off the detector nuclei placed at various underground laboratories. These scattering processes occur mainly through the exchange of the SM-like Higgs boson  $\chi_1$ . The Feynman diagrams for the spin independent scattering of both the dark matter particles with the detector nucleon ( $N$ ) are shown in Fig. 6. The expression for spin independent elastic scattering cross



Figure 6: Feynman diagrams for the spin independent elastic scattering between each of the dark matter particles and the nucleon ( $N$ ).

section between the dark matter component  $\chi_i$  ( $i = 2, 3$ ) and the nucleon  $N$  through the exchange of  $\chi_1$  is given by

$$\sigma_{SI}^{\chi_i N \rightarrow \chi_i N} = \frac{\mu_{Ni}^2}{\pi} \left( \frac{g_{\chi_1 \chi_i \chi_i}}{v} \right)^2 \left( \frac{M_N}{M_{\chi_i} M_{\chi_1}^2} \right)^2 f^2, \quad (29)$$

where  $\mu_{Ni}$  is the reduced mass between the dark matter component  $\chi_i$  and the nucleon  $N$  of mass  $M_N$ . In Eq. (29) the coupling term among the fields  $\chi_1 \chi_i \chi_i$  is represented by the quantity  $g_{\chi_1 \chi_i \chi_i}$  while  $f \sim 0.3$  [82] is the usual nucleonic matrix element. The expressions of the coupling term  $g_{\chi_1 \chi_i \chi_i}$  for  $i = 2, 3$  are given in Appendix A.1.

We have already shown that in the present scenario the dark sector is composed of two different scalar fields  $\chi_2$  and  $\chi_3$  whose masses as well as interaction strengths with the SM particles are different. Therefore in order to compare the spin independent scattering cross



section between each of the dark matter particles and the nucleon, computed using the present formalism with the results obtained from the present ongoing direct detection experiments such as XENON 100 [76], LUX [77], one needs to multiply the scattering cross section  $\sigma_{SI}^{\chi_i N \rightarrow \chi_i N}$  by the factor  $R_{\chi_i} = \frac{n_{\chi_i}}{n_{\chi_2} + n_{\chi_3}}$  [41], where  $n_{\chi_i}$  is the number density of the dark matter candidate  $\chi_i$ . The rescaling of  $\sigma_{SI}^{\chi_i N \rightarrow \chi_i N}$  is due to the fact that the exclusion plots obtained from various dark matter direct detection experiments are computed by assuming that the Universe contains only one type of dark matter particle, which is not a valid assumption for the present scenario. The spin independent scattering cross sections of both the dark matter particles  $\chi_2, \chi_3$  are given in Table 2. It is seen from Table 2 that the couplings for the vertices  $\chi_1 \chi_2 \chi_2$  and  $\chi_1 \chi_3 \chi_3$

Dark matter candidate ( $\chi_i$ )	Mass (GeV)	$g_{\chi_1 \chi_i \chi_i}$ (GeV)	$\sigma_{SI}^{\chi_i N \rightarrow \chi_i N}$ (pb)	$R_{\chi_i}$
$\chi_2$	50 – 80	$(0.44 - 3.9) \times 10^{-9}$	$(0.02 - 4.42) \times 10^{-27}$	$10^{-9} - 10^{-6}$
$\chi_3$	$7.1 \times 10^{-6}$	$(1.4 - 6.4) \times 10^{-7}$	$(0.14 - 3.03) \times 10^{-19}$	$\sim 1$

Table 2: Spin independent scattering cross sections of the dark matter particles  $\chi_2$  and  $\chi_3$ .

are extremely small (due to the nonthermal origin of  $\chi_2$  and  $\chi_3$ ). Hence the spin independent scattering cross sections of both the dark matter particles  $\chi_2$  and  $\chi_3$  lie well below the present limit which is  $\sim 10^{-9}$  pb to  $10^{-10}$  pb for a dark matter particle having mass in the range 10 GeV – 100 GeV [77].

## 6 $\gamma$ -ray excess at 1-3 GeV energies from Galactic Centre.

Our endeavour in this section is to explain, within the framework of our proposed two component dark matter model, the  $\gamma$ -ray excess from the Galactic Centre observed at an energy range 1 to 3 GeV by the Fermi-Large Area Telescope. One of our dark matter components, namely  $\chi_2$  having a mass in the range  $\sim 50$ –80 GeV, decays predominantly into the  $b\bar{b}$  final state since it has nonzero mixing with the SM-like Higgs boson  $\chi_1$ . The  $\chi_2 b\bar{b}$  coupling ( $g_{f f \chi_2}$ ,  $f = b$ ) can be read off from the expression given in Appendix A.1. It is noteworthy that the small strength of the  $\chi_1 \chi_2 \chi_2$  coupling makes the pair annihilation of two  $\chi_2$ ’s into  $b\bar{b}$  (through an s channel  $\chi_1$  exchange) a negligible competitor. We believe that ours is the first model explaining the Fermi-LAT  $\gamma$ -ray excess purely from the decay  $\chi_2 \rightarrow b\bar{b}$ . The b-quarks resulting from the decay of  $\chi_2$  hadronise to produce  $\gamma$ -rays, the spectrum of which should explain the 1-3 GeV excess as seen by Fermi-LAT. The differential  $\gamma$ -ray flux due to the decay of the component  $\chi_2$  in the

channel  $\chi_2 \rightarrow b\bar{b}$  in our two component DM model is given by [83]

$$\frac{d\Phi_\gamma}{d\Omega dE} = \frac{r_\odot}{4\pi} \frac{\rho_\odot}{M_{\chi_2}} \bar{J} \Gamma'_{\chi_2 \rightarrow b\bar{b}} \frac{dN_\gamma^b}{dE} . \quad (30)$$

In Eq. (30),  $\frac{dN_\gamma^b}{dE}$  is the energy spectrum of the photons produced with energy  $E$  from the hadronisation of  $b$  quarks<sup>7</sup>. We have used the numerical values of the photon spectrum ( $\frac{dN_\gamma^b}{dE}$ ) for different photon energies given in Ref. [83]. The value of the dark matter density at the solar location, namely  $\rho_\odot$ , is taken to be  $0.3 \text{ GeV/cm}^3$  while  $r_\odot \simeq 8.5 \text{ Kpc}$  is the distance between the GC and the solar location. We have averaged the  $J$  factor over the opening solid angles:

$$\bar{J} = \frac{4}{\Delta\Omega} \int \int db \, dl \cos b \, J(l, b) \quad (31)$$

with

$$J(l, b) = \int_{\text{l.o.s}} \frac{d\mathfrak{s}}{r_\odot} \left( \frac{\rho(r)}{\rho_\odot} \right) \quad (32)$$

and

$$\Omega = 4 \int dl \int db \cos b , \quad (33)$$

$$r = (r_\odot^2 + \mathfrak{s}^2 - 2 r_\odot \mathfrak{s} \cos b \cos l)^{1/2} . \quad (34)$$

In Eqs. (31), (33), (34),  $l$  and  $b$  denote the galactic longitude and latitude respectively and  $\mathfrak{s}$  is the line of sight distance. While computing the values of  $\bar{J}$ , we have performed the integral over a region which is situated within an angular distance of  $5^\circ$  [12] around the GC. The integral over  $\mathfrak{s}$  in Eq. (32) is along the line of sight (l.o.s). In the expression for differential  $\gamma$ -ray flux (Eq. (30)) the quantity  $\Gamma'_{\chi_2 \rightarrow b\bar{b}}$  is the product of the decay width of the channel  $\chi_2 \rightarrow b\bar{b}$  and the contribution of the component  $\chi_2$  to the total dark matter relic density ( $\Omega_{\text{T}} h^2$ ):

$$\Gamma'_{\chi_2 \rightarrow b\bar{b}} = \xi_{\chi_2} \Gamma_{\chi_2 \rightarrow b\bar{b}} , \quad (35)$$

where

$$\xi_{\chi_2} = \frac{\Omega_{\chi_2}}{\Omega_{\text{T}}} \quad (36)$$

is the fractional relic density for the component  $\chi_2$ . The use of the modified decay width  $\Gamma'_{\chi_2 \rightarrow b\bar{b}}$  (Eq. 35), instead of the actual decay width of the channel  $\chi_2 \rightarrow b\bar{b}$  ( $\Gamma_{\chi_2 \rightarrow b\bar{b}}$ ) in Eq. (30),

---

<sup>7</sup>These originate from the decay of the dark matter component  $\chi_2$  through the process  $\chi_2 \rightarrow b\bar{b}$ .

is required here as we are dealing with a two component dark matter model and the fractional amount of the relevant component should be considered for the computation. Needless to mention here that, if the entire dark sector consists of only one type of particle (say  $\chi_2$ ), then  $\xi_{\chi_2} = 1$ , and consequently  $\Gamma'_{\chi_2 \rightarrow b\bar{b}}$  and  $\Gamma_{\chi_2 \rightarrow b\bar{b}}$  are identical. We calculate the decay width of the DM component  $\chi_2$  for the  $b\bar{b}$  final state (see Fig. 7 for the Feynman diagram of this decay process) and the expression for this decay process is given below:

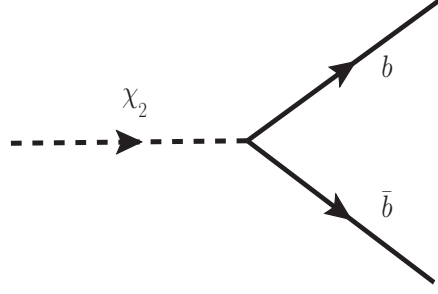


Figure 7: Feynman diagram for the decay channel  $\chi_2 \rightarrow b\bar{b}$ .

$$\Gamma_{\chi_2 \rightarrow b\bar{b}} = \frac{n_c G_F}{4\sqrt{2}\pi} (\sin \theta_{12} \cos \theta_{23} + \cos \theta_{12} \sin \theta_{23} \sin \theta_{13})^2 M_{\chi_2} M_b^2 \beta_b^3, \quad (37)$$

where

$$\beta_b = \left( 1 - \frac{4M_b^2}{M_{\chi_2}^2} \right)^{1/2}.$$

In the above,  $G_F = \frac{1}{\sqrt{2}v^2}$ , with  $v$  as defined in Eq. (1), is the Fermi constant and  $M_b$  is the mass of the  $b$  quark.

For the computation of the  $\gamma$ -ray flux using Eq. (30), the astrophysical input is the variation of dark matter density (as a function of the radial distance  $r$ ) in the neighbourhood of the GC. This functional relation between  $\rho(r)$  and  $r$  is known as the halo profile of DM. In this work, the computation of the gamma flux is done considering the NFW profile [75]. The general expression of the NFW profile is given by,

$$\rho_{\text{NFW}} = \rho_s \frac{\left( \frac{r}{r_s} \right)^{-\gamma}}{\left( 1 + \frac{r}{r_s} \right)^{3-\gamma}}, \quad (38)$$

where  $\gamma$  is a parameter (index) of order one. In the present calculation  $\gamma = 1$  is adopted. Now the halo profile reduces to the form

$$\rho_{\text{NFW}} = \rho_s \frac{\left( \frac{r_s}{r} \right)}{\left( 1 + \frac{r}{r_s} \right)^2}, \quad (39)$$

where  $r_s = 20$  Kpc. The normalisation constant  $\rho_s$  is obtained by demanding that the dark matter density at the solar location ( $r = r_\odot$ ) is  $0.3 \text{ GeV/cm}^3$ .

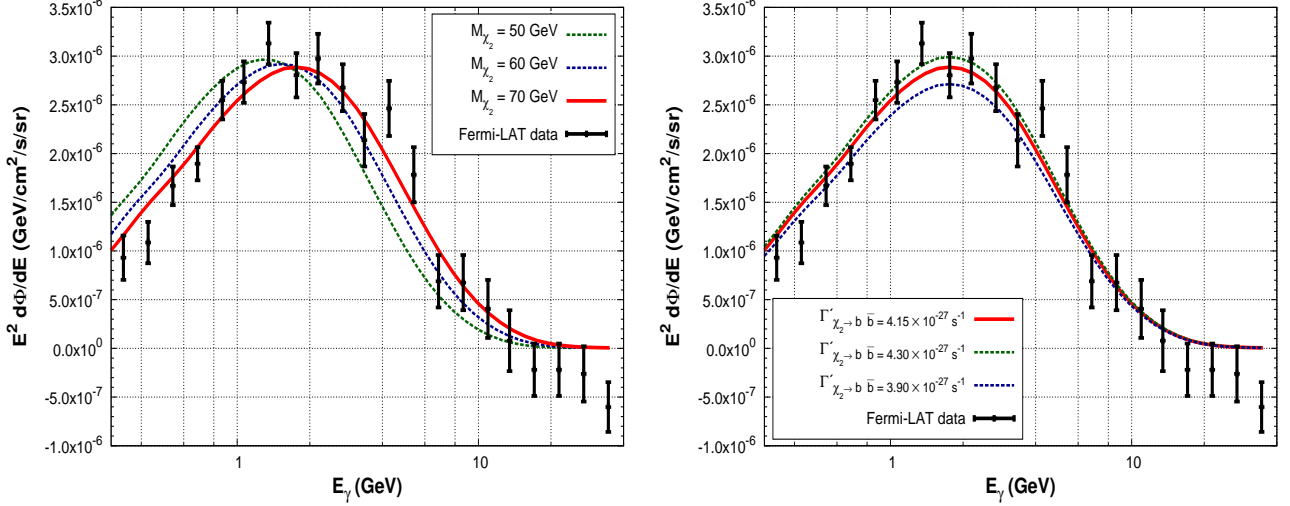


Figure 8: Left Panel:  $\gamma$ -ray flux for three different values of  $M_{\chi_2} = 50, 60, 70$  GeV. Right Panel:  $\gamma$ -ray flux obtained from the decay of a 70 GeV dark matter particle ( $\chi_2$ ) for three different values of modified decay width of the channel  $\chi_2 \rightarrow b\bar{b}$ .

The gamma-ray flux is calculated following the above discussion and the results are shown in Fig. 8. The Fermi-LAT observational results (black vertical lines) are shown in Fig. 8 for comparison. In the left panel of Fig. 8, we plot the  $\gamma$  flux from the Galactic Centre region for three values of  $\chi_2$  namely  $M_{\chi_2} = 50, 60, 70$  GeV. From the left panel of Fig. 8, it is evident that the Fermi-LAT results are best described for the choice  $M_{\chi_2} = 70$  GeV. In the right panel of Fig. 8, we adopt the value  $M_{\chi_2} = 70$  GeV and compare our calculated results (for the  $\gamma$  flux) with the Fermi-LAT observational data with three different values of modified decay widths  $\Gamma'_{\chi_2 \rightarrow b\bar{b}} = 3.90 \times 10^{-27} \text{ s}^{-1}$  (blue dashed line),  $4.15 \times 10^{-27} \text{ s}^{-1}$  (red solid line) and  $4.30 \times 10^{-27} \text{ s}^{-1}$  (green dashed line) respectively for the process  $\chi_2 \rightarrow b\bar{b}$ . The right panel of Fig. 8 shows that the decay width of  $\Gamma'_{\chi_2 \rightarrow b\bar{b}} = 4.15 \times 10^{-27} \text{ s}^{-1}$  best represents the observational results from Fermi-LAT. Here we note that obtaining  $\Gamma'_{\chi_2 \rightarrow b\bar{b}}$  in the right ballpark of  $3.90 \times 10^{-27} \text{ s}^{-1}$  to  $4.30 \times 10^{-27} \text{ s}^{-1}$ , one requires the soft breaking parameter  $\alpha$  to be in the range  $10^{-9} \text{ GeV}^2 \lesssim \alpha \lesssim 10^{-7} \text{ GeV}^2$ .

We had mentioned earlier that we have taken the canonical NFW profile where the index  $\gamma$  equals 1 in Eq. (39). But in Ref. [12], where a model independent analysis of Fermi-LAT data with dark matter annihilation has been made to explain the gamma excess in the energy region 1-3 GeV, a profile steeper than the canonical NFW profile with  $\gamma = 1.26$  was taken. The index  $\gamma \sim 1.2$  was also required for explaining, within the framework of dark matter annihilation, the

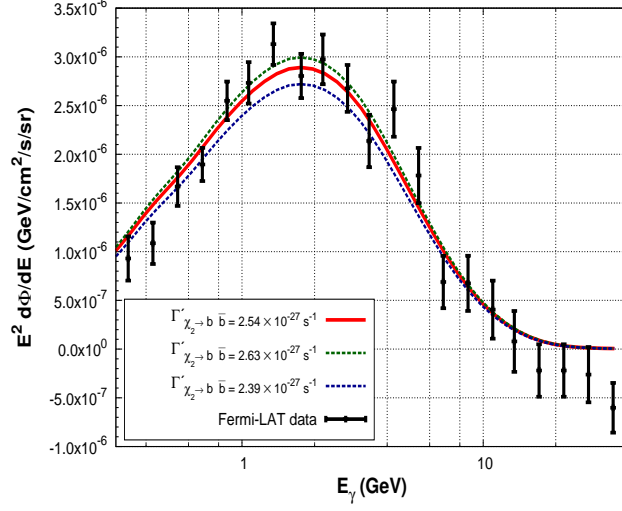


Figure 9:  $\gamma$ -ray flux obtained from the decay of a 70 GeV dark matter particle ( $\chi_2$ ) for a steeper NFW profile with  $\gamma = 1.26$ . Three lines represent the  $\gamma$ -ray flux for three different values of modified decay width of the channel  $\chi_2 \rightarrow b\bar{b}$ .

gamma signal from the Fermi bubble region in Ref. [10]. We therefore also compute the gamma flux from the Galactic Centre in the present framework using a steeper NFW profile with index  $\gamma = 1.26$ . The results are shown in Fig. 9 where we plot the calculated gamma ray flux (taking an NFW type profile where  $\gamma = 1.26$ ) with  $M_{\chi_2} = 70$  GeV and three values of the modified decay width  $\Gamma'_{\chi_2 \rightarrow b\bar{b}}$ . In this case the Fermi-LAT data are best represented when  $\Gamma'_{\chi_2 \rightarrow b\bar{b}} = 2.54 \times 10^{-27} \text{ s}^{-1}$ .

## 7 3.55 keV X-ray line

We mentioned earlier that our present two component dark matter model contains a scalar particle  $\chi_3$ , with a mass of order keV, which possesses a tiny mixing with the SM-like Higgs boson  $\chi_1$ . The two photon decay mode of the dark matter candidate  $\chi_3$  produces monoenergetic photons (X-rays) which have been detected by the X-ray telescopes of the XMM-Newton observatory. It has been reported in Refs. [3, 4, 66] that, in order to produce the observed X-ray flux from the decay of a dark matter particle, the corresponding decay width for the channel  $\text{DM} \rightarrow \gamma\gamma$  must be in the range  $\sim 2.5 \times 10^{-29} \text{ s}^{-1}$  to  $2.5 \times 10^{-28} \text{ s}^{-1}$ . In the present scenario, the above constraint should be applied on the modified decay width instead of the actual decay width ( $\Gamma_{\chi_3 \rightarrow \gamma\gamma}$ ) for the channel  $\chi_3 \rightarrow \gamma\gamma$ , since we are working in a framework where the entire dark sector is composed of two different scalar fields  $\chi_2$  and  $\chi_3$ . The modified decay width ( $\Gamma'_{\chi_3 \rightarrow \gamma\gamma}$ ) of  $\chi_3$  for the channel

$\chi_3 \rightarrow \gamma\gamma$  is defined as,

$$\Gamma'_{\chi_3 \rightarrow \gamma\gamma} = \xi_{\chi_3} \Gamma_{\chi_3 \rightarrow \gamma\gamma} \quad (40)$$

with

$$\xi_{\chi_3} = \frac{\Omega_{\chi_3}}{\Omega_T} \quad (41)$$

as the fractional contribution of the DM component  $\chi_3$  to the total relic density ( $\Omega_T h^2$ ). The Feynman diagrams for the decay channel  $\chi_3 \rightarrow \gamma\gamma$  are shown in Fig. 10. The expression for the

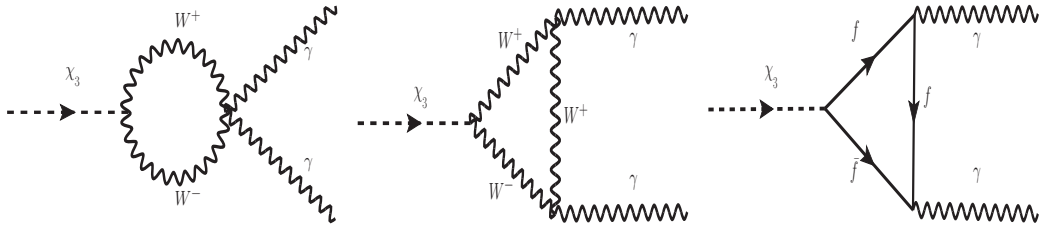


Figure 10: One loop Feynman diagrams for the decay channel  $\chi_3 \rightarrow \gamma\gamma$ .

decay width for the channel  $\chi_3 \rightarrow \gamma\gamma$ , which takes place at one loop, is given by

$$\Gamma_{\chi_3 \rightarrow \gamma\gamma} = \frac{G_F m_{\chi_3}^3 \alpha_{\text{em}}^2}{128\sqrt{2} \pi^3} (\sin \theta_{12} \sin \theta_{23} - \cos \theta_{12} \cos \theta_{23} \sin \theta_{13})^2 |F|^2, \quad (42)$$

where

$$F = F_W(\tau_W) + \sum_f n_{cf} Q_f^2 F_f(\tau_f) \quad (43)$$

with

$$\begin{aligned} \tau_W &= \frac{4M_W^2}{M_{\chi_3}^2}, \quad \tau_f = \frac{4M_f^2}{M_{\chi_3}^2}, \\ F_W(\tau_W) &= 2 + 3\tau_W + 3\tau_W(2 - \tau_W)\mathfrak{g}(\tau_W), \\ F_f(\tau_f) &= -2\tau_f[1 + (1 - \tau_f)\mathfrak{g}(\tau_f)], \\ \mathfrak{g}(\tau) &= \arcsin^2[\tau^{-1/2}]. \end{aligned} \quad (44)$$

Here  $\alpha_{\text{em}} \simeq \frac{1}{137}$  is the fine structure constant while  $Q_f$  and  $n_{cf}$  are the electric charge and the colour charge of the fermion ( $f$ )<sup>8</sup> involved in the fermionic loop of Fig. 10.

---

<sup>8</sup> $f$  is any SM fermion

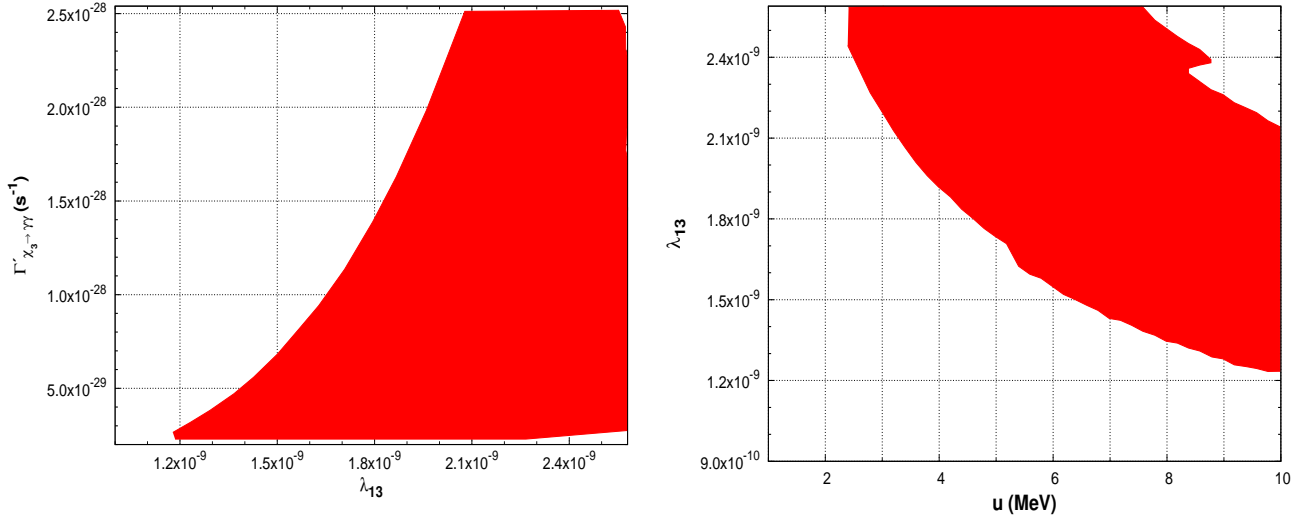


Figure 11: Left panel: Variation of the modified decay width  $\Gamma'_{\chi_3 \rightarrow \gamma\gamma}$  of the decay channel  $\chi_3 \rightarrow \gamma\gamma$  with  $\lambda_{13}$ . Right panel: Allowed region in the  $u - \lambda_{13}$  plane which produces the observed X-ray flux as well as satisfies the PLANCK limit on the total relic density.

In the left panel of Fig. 11 we show the allowed range  $1.2 \times 10^{-9} \lesssim \lambda_{13} \lesssim 2.6 \times 10^{-9}$  of the parameter  $\lambda_{13}$  for which the modified decay width ( $\Gamma'_{\chi_3 \rightarrow \gamma\gamma}$ ) for the decay channel  $\chi_3 \rightarrow \gamma\gamma$  lies in the range  $2.5 \times 10^{-29} \leq \Gamma'_{\chi_3 \rightarrow \gamma\gamma}(\text{s}^{-1}) \leq 2.5 \times 10^{-28}$  which is necessary to produce the observed X-ray flux from the extragalactic sources such as Perseus, Andromeda etc. The right panel of Fig. 11 shows the allowed region in the  $u - \lambda_{13}$  plane. From this plot (right panel of Fig. 11) one notices that, in order to produce the observed X-ray flux, the VEV  $u$  of the scalar field  $S_3$  must be  $> 2.4$  MeV. The upper bound ( $u \leq 10$  MeV) on the allowed values of  $u$  comes from the domain wall constraint (see Section 3.4 of Ref. [57]) which arises from the spontaneous breaking of the discrete symmetry  $\mathbb{Z}_2''$ . Needless to mention here that, for all the points in both panels of Fig. 11, the PLANCK limit on total relic density  $\Omega_{\text{T}} h^2$  of the dark matter candidates is always satisfied.

## 8 Conclusion

In this paper we have presented a two-component model of nonthermal dark matter by postulating two additional SM-singlet scalar fields  $S_2$  and  $S_3$  which interact among themselves and with the SM Higgs doublet  $H$ . These interaction terms have been restricted by assuming a suitable  $\mathbb{Z}_2 \times \mathbb{Z}_2'$  discrete symmetry which is softly and explicitly broken to a residual  $\mathbb{Z}_2''$  symmetry. The latter gets spontaneously broken when  $S_3$  develops a VEV of order MeV. Our physical scalar

spectrum comprises three particles: (1) the SM-like Higgs boson  $\chi_1$  with  $M_{\chi_1} \sim 125$  GeV, (2) a moderately heavy scalar dark matter particle  $\chi_2$  with  $50 \text{ GeV} \leq M_{\chi_2} \leq 80 \text{ GeV}$  and (3) a very light scalar DM particle  $\chi_3$  with  $M_{\chi_3} \sim 7 \text{ keV}$ . We have discussed the issue of domain wall formation which arises in our model due to spontaneous breaking of the discrete symmetry  $\mathbb{Z}_2''$  and have explained why it is unimportant for us. We have computed the  $\gamma$ -ray flux from the decay channel  $\chi_2 \rightarrow b\bar{b}$  of the heavier dark matter candidate  $\chi_2$  while the X-ray line is generated from the decay mode of the lighter DM candidate  $\chi_3$  into a pair of two keV energy photons. These two decay channels ( $\chi_2 \rightarrow b\bar{b}$ ,  $\chi_3 \rightarrow \gamma\gamma$ ) exist due to the fact that both the DM candidates in the present scenario possess tiny amounts of mixing with the SM-like Higgs boson  $\chi_1$ . We have found that the  $\gamma$ -ray flux originating from the decay of a 70 GeV dark matter particle ( $\chi_2$ ) into a  $b\bar{b}$  final state at the Galactic Centre with a modified decay width  $\Gamma'_{\chi_2 \rightarrow b\bar{b}} = 4.15 \times 10^{-27} \text{ s}^{-1}$  fits the Fermi-LAT data well. Finally, we have shown that the modified decay width of the lighter dark matter component  $\chi_3$  for the channel  $\chi_3 \rightarrow \gamma\gamma$  lies in the appropriate range of  $2.5 \times 10^{-29} \text{ s}^{-1}$  to  $2.5 \times 10^{-28} \text{ s}^{-1}$  as long as the VEV  $u$  is bounded from below by 2.4 MeV.

## 9 Acknowledgement

One of the authors A.B. would like to thank D. Adak, M. Chakraborty, A. Dutta Banik and N. Haque for many useful suggestions and discussions. The research of A.B. has been funded by the Department of Atomic Energy (DAE) of Govt. of India. P.R. has been supported as a Senior Scientist by the Indian National Science Academy.





# A Appendix

## A.1 Couplings of the physical scalars $\chi_1$ , $\chi_2$ and $\chi_3$

The couplings of the physical scalars  $\chi_1$ ,  $\chi_2$ ,  $\chi_3$  – among themselves and with other SM particles are – given below in the limit when all three mixing angles  $\theta_{12}$ ,  $\theta_{13}$ ,  $\theta_{23}$  are extremely small.

$$\begin{aligned}
g_{\chi_1 \chi_1 \chi_2 \chi_2} &\simeq -\theta_{23}(3\theta_{12}\theta_{13}\kappa_1 - 3\theta_{12}\theta_{13}\lambda_{12} - 2\theta_{12}\theta_{13}\lambda_{13} + 4\theta_{12}\theta_{13}\lambda_{23}) - \frac{\lambda_{12}}{2} , \\
g_{\chi_1 \chi_1 \chi_3 \chi_3} &\simeq -\theta_{23}(-3\theta_{12}\theta_{13}\kappa_1 + 3\theta_{12}\theta_{13}\lambda_{12} + 2\theta_{12}\theta_{13}\lambda_{13} - 4\theta_{12}\theta_{13}\lambda_{23}) - \frac{\lambda_{13}}{2} , \\
g_{\chi_2 \chi_2 \chi_3 \chi_3} &\simeq -\lambda_{23} - \theta_{23}(3\theta_{12}\theta_{13}\kappa_2 - 3\theta_{12}\theta_{13}\lambda_{12} + 3\theta_{12}\theta_{13}\lambda_{13} - 6\theta_{12}\theta_{13}\lambda_{23}) , \\
g_{\chi_1 \chi_1 \chi_1} &\simeq -v\kappa_1 - \theta_{13}u\lambda_{13} , \\
g_{\chi_2 \chi_2 \chi_2} &\simeq \theta_{12}v\lambda_{12} - \theta_{23}(2u\lambda_{23} - \theta_{13}v\lambda_{12}) , \\
g_{\chi_3 \chi_3 \chi_3} &\simeq -u\kappa_3 + \theta_{13}v\lambda_{13} - \theta_{23}(-2\theta_{12}\theta_{13}u\lambda_{13} + \theta_{12}v\lambda_{13} + 4\theta_{12}\theta_{13}u\lambda_{23}) , \\
g_{\chi_1 \chi_2 \chi_2} &\simeq -\theta_{23}(6\theta_{12}\theta_{13}v\kappa_1 - 4\theta_{12}\theta_{13}v\lambda_{12} - 2\theta_{12}u\lambda_{13} - 2\theta_{12}\theta_{13}v\lambda_{13} + 4\theta_{12}u\lambda_{23}) \\
&\quad - v\lambda_{12} - 2\theta_{13}u\lambda_{23} \\
g_{\chi_1 \chi_3 \chi_3} &\simeq -\theta_{23}(-6\theta_{12}\theta_{13}v\kappa_1 + 4\theta_{12}\theta_{13}v\lambda_{12} + 2\theta_{12}u\lambda_{13} + 2\theta_{12}\theta_{13}v\lambda_{13} - 4\theta_{12}u\lambda_{23}) \\
&\quad - v\lambda_{13} + 2\theta_{13}u\lambda_{13} - 3\theta_{13}u\kappa_3 \\
g_{\chi_2 \chi_3 \chi_3} &\simeq -\theta_{23}(3u\kappa_3 + 2\theta_{13}v\lambda_{12} - 3\theta_{13}v\lambda_{13} - 4u\lambda_{23}) - 2\theta_{12}\theta_{13}u\lambda_{13} + \theta_{12}v\lambda_{13} \\
&\quad + 4\theta_{12}\theta_{13}u\lambda_{23} , \\
g_{\chi_1 \chi_2 \chi_3} &\simeq -\theta_{23}(6\theta_{13}u\kappa_3 - 2v\lambda_{12} - 4\theta_{13}u\lambda_{13} + 2v\lambda_{13} - 4\theta_{13}u\lambda_{23}) - 6\theta_{12}\theta_{13}v\kappa_1 \\
&\quad + 4\theta_{12}\theta_{13}v\lambda_{12} + 2\theta_{12}u\lambda_{13} + 2\theta_{12}\theta_{13}v\lambda_{13} - 4\theta_{12}u\lambda_{23} , \\
g_{WW\chi_1} &\simeq \frac{2M_W^2}{v} , \\
g_{WW\chi_2} &\simeq -\frac{2M_W^2}{v}(\theta_{12} + \theta_{13}\theta_{23}) , \\
g_{WW\chi_3} &\simeq -\frac{2M_W^2}{v}(\theta_{13} - \theta_{12}\theta_{23}) , \\
g_{ZZ\chi_1} &\simeq \frac{M_W^2}{v} , \\
g_{ZZ\chi_2} &\simeq -\frac{M_W^2}{v}(\theta_{12} + \theta_{13}\theta_{23}) , \\
g_{ZZ\chi_3} &\simeq -\frac{M_W^2}{v}(\theta_{13} - \theta_{12}\theta_{23}) , \\
g_{ff\chi_1} &\simeq -\frac{M_f}{v} , \\
g_{ff\chi_2} &\simeq \frac{M_f}{v}(\theta_{12} + \theta_{13}\theta_{23}) , \\
g_{ff\chi_3} &\simeq \frac{M_f}{v}(\theta_{13} - \theta_{12}\theta_{23}) .
\end{aligned}$$

## A.2 Masses of physical scalars $\chi_1$ , $\chi_2$ and $\chi_3$

The masses of the physical scalar  $\chi_1$ ,  $\chi_2$  and  $\chi_3$  in the limit of extremely small  $\theta_{12}$ ,  $\theta_{13}$ ,  $\theta_{23}$  are given as follows:

$$M_{\chi_1} = (2\kappa_1 v^2 + 4uv\theta_{13}\lambda_{13} + 2\alpha\theta_{12}\theta_{13})^{1/2} + \mathcal{O}(\theta_{12}^2) + \mathcal{O}(\theta_{23}^2) + \mathcal{O}(\theta_{13}^2) ,$$

$$M_{\chi_2} = \left\{ \rho_2^2 + \lambda_{12}v^2 + 2\lambda_{23}u^2 + 2\theta_{23} \left( \alpha - \rho_2^2\theta_{12}\theta_{13} + 2v^2\kappa_1\theta_{12}\theta_{13} - v^2\lambda_{12}\theta_{12}\theta_{13} \right. \right. \\ \left. \left. - 2uv\lambda_{13}\theta_{12} - 2u^2\lambda_{23}\theta_{12}\theta_{13} \right) \right\}^{1/2} + \mathcal{O}(\theta_{12}^2) + \mathcal{O}(\theta_{23}^2) + \mathcal{O}(\theta_{13}^2) ,$$

$$M_{\chi_3} = \left\{ 2\kappa_3 u^2 - 2\alpha\theta_{12}\theta_{13} - 4uv\theta_{13}\lambda_{13} - 2\theta_{23} \left( \alpha - \rho_2^2\theta_{12}\theta_{13} + 2v^2\kappa_1\theta_{12}\theta_{13} \right. \right. \\ \left. \left. - v^2\lambda_{12}\theta_{12}\theta_{13} - 2uv\lambda_{13}\theta_{12} - 2u^2\lambda_{23}\theta_{12}\theta_{13} \right) \right\}^{1/2} + \mathcal{O}(\theta_{12}^2) + \mathcal{O}(\theta_{23}^2) + \mathcal{O}(\theta_{13}^2) .$$

## References

- [1] G. Bertone, D. Hooper and J. Silk, Phys. Rept. **405**, 279 (2005) [hep-ph/0404175].
- [2] P. A. R. Ade *et al.* [Planck Collaboration], Astron. Astrophys. **571**, A16 (2014) [arXiv:1303.5076 [astro-ph.CO]].
- [3] E. Bulbul, M. Markevitch, A. Foster, R. K. Smith, M. Loewenstein and S. W. Randall, Astrophys. J. **789**, 13 (2014) [arXiv:1402.2301 [astro-ph.CO]].
- [4] A. Boyarsky, O. Ruchayskiy, D. Iakubovskiy and J. Franse, Phys. Rev. Lett. **113**, 251301 (2014) [arXiv:1402.4119 [astro-ph.CO]].
- [5] L. Goodenough and D. Hooper, arXiv:0910.2998 [hep-ph].
- [6] D. Hooper and L. Goodenough, Phys.Lett. **B697** (2011) 412–428, arXiv:1010.2752 [hep-ph].
- [7] A. Boyarsky, D. Malyshev, and O. Ruchayskiy, Phys.Lett. **B705** (2011) 165–169, arXiv:1012.5839 [hep-ph].
- [8] D. Hooper and T. Linden, Phys.Rev. **D84** (2011) 123005, arXiv:1110.0006 [astro-ph.HE].
- [9] K. N. Abazajian and M. Kaplinghat, Phys.Rev. **D86** (2012) 083511, arXiv:1207.6047 [astro-ph.HE].
- [10] D. Hooper and T. R. Slatyer, Phys.Dark Univ. **2** (2013) 118–138, arXiv:1302.6589 [astro-ph.HE].

- [11] K. N. Abazajian, N. Canac, S. Horiuchi, and M. Kaplinghat, Phys.Rev. **D90** (2014) 023526, arXiv:1402.4090 [astro-ph.HE].
- [12] T. Daylan, D. P. Finkbeiner, D. Hooper, T. Linden, S. K. N. Portillo, et al., arXiv:1402.6703 [astro-ph.HE].
- [13] P. Agrawal, B. Batell, P. J. Fox and R. Harnik, arXiv:1411.2592 [hep-ph].
- [14] F. Calore, I. Cholis, C. McCabe and C. Weniger, arXiv:1411.4647 [hep-ph].
- [15] T. E. Jeltema and S. Profumo, arXiv:1408.1699 [astro-ph.HE].
- [16] E. Carlson, T. Jeltema and S. Profumo, JCAP **1502**, no. 02, 009 (2015) [arXiv:1411.1758 [astro-ph.HE]].
- [17] D. Malyshev, A. Neronov and D. Eckert, Phys. Rev. D **90**, no. 10, 103506 (2014) [arXiv:1408.3531 [astro-ph.HE]].
- [18] M. E. Anderson, E. Churazov and J. N. Bregman, arXiv:1408.4115 [astro-ph.HE].
- [19] J. Petrovic, P. D. Serpico and G. Zaharijas, JCAP **1410**, no. 10, 052 (2014) [arXiv:1405.7928 [astro-ph.HE]].
- [20] J. Petrović, P. D. Serpico and G. Zaharijas, JCAP **1502**, no. 02, 023 (2015) [arXiv:1411.2980 [astro-ph.HE]].
- [21] M. S. Boucenna and S. Profumo, Phys. Rev. D **84**, 055011 (2011) [arXiv:1106.3368 [hep-ph]].
- [22] J. D. Ruiz-Alvarez, C. A. de S.Pires, F. S. Queiroz, D. Restrepo and P. S. Rodrigues da Silva, Phys. Rev. D **86**, 075011 (2012) [arXiv:1206.5779 [hep-ph]].
- [23] A. Alves, S. Profumo, F. S. Queiroz and W. Shepherd, Phys. Rev. D **90**, no. 11, 115003 (2014) [arXiv:1403.5027 [hep-ph]].
- [24] A. Berlin, D. Hooper and S. D. McDermott, Phys. Rev. D **89**, 115022 (2014) [arXiv:1404.0022 [hep-ph]].
- [25] P. Agrawal, B. Batell, D. Hooper and T. Lin, Phys. Rev. D **90**, 063512 (2014) [arXiv:1404.1373 [hep-ph]].
- [26] E. Izaguirre, G. Krnjaic and B. Shuve, Phys. Rev. D **90**, 055002 (2014) [arXiv:1404.2018 [hep-ph]].

- [27] D. G. Cerdeño, M. Peiró and S. Robles, JCAP **1408**, 005 (2014) [arXiv:1404.2572 [hep-ph]].
- [28] S. Ipek, D. McKeen and A. E. Nelson, Phys. Rev. D **90**, 055021 (2014) [arXiv:1404.3716 [hep-ph]].
- [29] C. Boehm, M. J. Dolan and C. McCabe, Phys. Rev. D **90**, 023531 (2014) [arXiv:1404.4977 [hep-ph]].
- [30] P. Ko, W. I. Park and Y. Tang, JCAP **1409**, 013 (2014) [arXiv:1404.5257 [hep-ph]].
- [31] M. Abdullah, A. DiFranzo, A. Rajaraman, T. M. P. Tait, P. Tanedo and A. M. Wijangco, Phys. Rev. D **90**, no. 3, 035004 (2014) [arXiv:1404.6528 [hep-ph]].
- [32] D. K. Ghosh, S. Mondal and I. Saha, arXiv:1405.0206 [hep-ph].
- [33] A. Martin, J. Shelton and J. Unwin, Phys. Rev. D **90**, no. 10, 103513 (2014) [arXiv:1405.0272 [hep-ph]].
- [34] L. Wang, arXiv:1406.3598 [hep-ph].
- [35] T. Basak and T. Mondal, arXiv:1405.4877 [hep-ph].
- [36] W. Detmold, M. McCullough and A. Pochinsky, Phys. Rev. D **90**, 115013 (2014) [arXiv:1406.2276 [hep-ph]].
- [37] C. Arina, E. Del Nobile and P. Panci, arXiv:1406.5542 [hep-ph].
- [38] N. Okada and O. Seto, Phys. Rev. D **90**, no. 8, 083523 (2014) [arXiv:1408.2583 [hep-ph]].
- [39] K. Ghorbani, arXiv:1408.4929 [hep-ph].
- [40] A. D. Banik and D. Majumdar, arXiv:1408.5795 [hep-ph].
- [41] A. Biswas, arXiv:1412.1663 [hep-ph].
- [42] K. Ghorbani and H. Ghorbani, arXiv:1501.00206 [hep-ph].
- [43] D. G. Cerdeno, M. Peiro and S. Robles, arXiv:1501.01296 [hep-ph].
- [44] R. Krall, M. Reece and T. Roxlo, JCAP **1409**, 007 (2014) [arXiv:1403.1240 [hep-ph]].
- [45] J. C. Park, S. C. Park and K. Kong, Phys. Lett. B **733**, 217 (2014) [arXiv:1403.1536 [hep-ph]].

- [46] M. T. Frandsen, F. Sannino, I. M. Shoemaker and O. Svendsen, JCAP **1405**, 033 (2014) [arXiv:1403.1570 [hep-ph]].
- [47] S. Baek and H. Okada, arXiv:1403.1710 [hep-ph].
- [48] K. Nakayama, F. Takahashi and T. T. Yanagida, Phys. Lett. B **735**, 338 (2014) [arXiv:1403.1733 [hep-ph]].
- [49] K. Y. Choi and O. Seto, Phys. Lett. B **735**, 92 (2014) [arXiv:1403.1782 [hep-ph]].
- [50] M. Cicoli, J. P. Conlon, M. C. D. Marsh and M. Rummel, Phys. Rev. D **90**, no. 2, 023540 (2014) [arXiv:1403.2370 [hep-ph]].
- [51] C. Kolda and J. Unwin, Phys. Rev. D **90**, 023535 (2014) [arXiv:1403.5580 [hep-ph]].
- [52] R. Allahverdi, B. Dutta and Y. Gao, Phys. Rev. D **89**, 127305 (2014) [arXiv:1403.5717 [hep-ph]].
- [53] N.-E. Bomark and L. Roszkowski, Phys. Rev. D **90**, no. 1, 011701 (2014) [arXiv:1403.6503 [hep-ph]].
- [54] S. P. Liew, JCAP **1405**, 044 (2014) [arXiv:1403.6621 [hep-ph]].
- [55] K. Nakayama, F. Takahashi and T. T. Yanagida, Phys. Lett. B **734**, 178 (2014) [arXiv:1403.7390 [hep-ph]].
- [56] E. Dudas, L. Heurtier and Y. Mambrini, Phys. Rev. D **90**, 035002 (2014) [arXiv:1404.1927 [hep-ph]].
- [57] K. S. Babu and R. N. Mohapatra, Phys. Rev. D **89**, 115011 (2014) [arXiv:1404.2220 [hep-ph]].
- [58] K. P. Modak, arXiv:1404.3676 [hep-ph].
- [59] S. Baek, P. Ko and W. I. Park, arXiv:1405.3730 [hep-ph].
- [60] S. Chakraborty, D. K. Ghosh and S. Roy, JHEP **1410**, 146 (2014) [arXiv:1405.6967 [hep-ph]].
- [61] C. W. Chiang and T. Yamada, JHEP **1409**, 006 (2014) [arXiv:1407.0460 [hep-ph]].
- [62] B. Dutta, I. Gogoladze, R. Khalid and Q. Shafi, JHEP **1411**, 018 (2014) [arXiv:1407.0863 [hep-ph]].

- [63] N. Haba, H. Ishida and R. Takahashi, arXiv:1407.6827 [hep-ph].
- [64] J. M. Cline and A. R. Frey, JCAP **1410**, no. 10, 013 (2014) [arXiv:1408.0233 [hep-ph]].
- [65] Y. Farzan and A. R. Akbarieh, JCAP **1411**, no. 11, 015 (2014) [arXiv:1408.2950 [hep-ph]].
- [66] T. Higaki, N. Kitajima and F. Takahashi, arXiv:1408.3936 [hep-ph].
- [67] S. Patra, N. Sahoo and N. Sahu, arXiv:1412.4253 [hep-ph].
- [68] K. S. Babu, S. Chakdar and R. N. Mohapatra, arXiv:1412.7745 [hep-ph].
- [69] K. Cheung, W. C. Huang and Y. L. S. Tsai, arXiv:1411.2619 [hep-ph].
- [70] Q. H. Cao, E. Ma, J. Wudka and C.-P. Yuan, arXiv:0711.3881 [hep-ph].
- [71] D. Feldman, Z. Liu, P. Nath and G. Peim, Phys. Rev. D **81**, 095017 (2010) [arXiv:1004.0649 [hep-ph]].
- [72] A. Biswas, D. Majumdar, A. Sil and P. Bhattacharjee, JCAP **1312**, 049 (2013) [arXiv:1301.3668 [hep-ph]].
- [73] S. Bhattacharya, A. Drozd, B. Grzadkowski and J. Wudka, JHEP **1310**, 158 (2013) [arXiv:1309.2986 [hep-ph]].
- [74] L. Bian, T. Li, J. Shu and X. C. Wang, arXiv:1412.5443 [hep-ph].
- [75] J. F. Navarro, C. S. Frenk and S. D. M. White, Astrophys. J. **490**, 493 (1997) [astro-ph/9611107].
- [76] E. Aprile *et al.* [XENON100 Collaboration], Phys. Rev. Lett. **109**, 181301 (2012) [arXiv:1207.5988 [astro-ph.CO]].
- [77] D. S. Akerib *et al.* [LUX Collaboration], Phys. Rev. Lett. **112**, no. 9, 091303 (2014) [arXiv:1310.8214 [astro-ph.CO]].
- [78] K. Kannike, Eur. Phys. J. C **72**, 2093 (2012) [arXiv:1205.3781 [hep-ph]].
- [79] J. Edsjo and P. Gondolo, Phys. Rev. D **56**, 1879 (1997) [hep-ph/9704361].
- [80] A. Biswas and D. Majumdar, Pramana **80**, 539 (2013) [arXiv:1102.3024 [hep-ph]].
- [81] L. Dolan and R. Jackiw, Phys. Rev. D **9**, 3320 (1974).

- [82] R. Barbieri, L. J. Hall and V. S. Rychkov, Phys. Rev. D **74**, 015007 (2006) [hep-ph/0603188].
- [83] M. Cirelli, G. Corcella, A. Hektor, G. Hutsi, M. Kadastik, P. Panci, M. Raidal and F. Sala *et al.*, JCAP **1103**, 051 (2011) [Erratum-ibid. **1210**, E01 (2012)] [arXiv:1012.4515 [hep-ph], arXiv:1012.4515 [hep-ph]].